REVISION 2

Cation arrangement in the octahedral and tetrahedral sheets of cis-vacant polymorph of dioctahedral 2:1 phyllosilicates by quantum mechanical calculations

E. ESCAMILLA-ROA[a], A. HERNÁNDEZ-LAGUNA[b], and C. IGNACIO SAINZ-DÍAZ[b *]

[a] Instituto de Astrofísica de Andalucía (CSIC), Glorieta de la Astronomía s/n, 18008 Granada (Spain).

[b] Instituto Andaluz de Ciencias de la Tierra (CSIC-UGR), Avda Las Palmeras 4, 18100 Armilla, Granada (Spain).

* Corresponding author: ignacio.sainz@iact.ugr-csic.es

Abstract

Density Functional Theory (DFT) calculations were performed to study the crystallographic properties of the cis-vacant form of dioctahedral 2:1 phyllosilicates. Samples with different layer charges are studied; only tetrahedrally charged, only octahedrally charged, or mixed octahedrally/tetrahedrally charged. The isomorphous cation substitutions were explored in different relative positions with substitutions of octahedral Al^{3+} by Mg^{2+} or Fe^{3+}, tetrahedral substitution of Si^{4+} by Al^{3+}, and different interlayer cations (IC) (Na^{+}, K^{+}, and Ca^{2+}). X-Ray diffraction patterns of cis-vacant and trans-vacant forms of phyllosilicates were simulated and compared. The experimental observation of clustering tendency of Fe^{3+} and dispersion tendency of Mg^{2+} in the octahedral sheet is reproduced and explained with reference to the relative energies of the octahedral cation arrangements observing the same tendency that in the trans-vacant forms. These energies are higher than those due to the IC/tetrahedral and IC/octahedral relative arrangements. The tetrahedral and octahedral substitutions that generate charged layers tend also to be dispersed. The energy difference between the cis-vacant and trans-vacant polymorphs is smaller than that of cation arrangements.

Keywords: DFT, clays, cation-ordering, phyllosilicate, polymorph, cis-vacant.

Introduction

Phyllosilicates are part of clay minerals, being one the main components of the Earth crust in soils and rocks. These minerals have also several technological uses as materials in catalytic chemistry and green technologies (adsorption of pollutants and treatment of industrial wastewaters). Besides, the adsorption and catalytic properties of these minerals make to consider the clays as support for the origin of the live on Earth and prebiotic reactions under hydrothermal conditions in sea-floors (Bernal, 1949; Swadling et al. 2010). On the other hand, clay minerals have been detected in carbonaceous chondrites of meteorites (Tagish Lake) (Herd et al., 2011), comets, asteroids, Mars (Mustard et al. 2008) and some satellites of the Solar System (Hibbitts and Szanyi, 2007; Lebofsky et al., 1982; Rubin, 1997). The distribution of these minerals in the asteroid belt can provide some clues to explain the conditions in which the solar system was originated.

The 2:1 phyllosilicates have a layered structure and consist of an octahedral (Oct) sheet sandwiched between two tetrahedral (T) sheets. The T sheet is formed by tetrahedra of SiO_4 and the Oct sheet is formed by octahedra of Al oxides. The T sheets are always bonded to Oct sheets through oxygen atoms. The Oct sheet has unshared oxygen atoms forming OH groups. On the other hand, in dioctahedral phyllosilicates, one out of three octahedral positions is not occupied by cations, forming a vacant site. The OH groups determine two kinds of crystal forms depending on their disposition in the vacant site of the octahedral sheet, i.e. when the OH groups can be on the same side (cis-vacant, cv) or on opposite sides (trans-vacant, tv) of the vacant site (Fig. 1). These cis-vacant/trans-vacant configurations were first reported by Méring and Oberlin (1971) in montmorrillonite. Drits et al. (1984) were the first to distinguish the reflections of each configuration and to deduce the crystal structure of a cv illite model. However,

Drits and Zviagina (2009) noted that in the powder XRD patterns of trans-vacant 3T (3T-tv) and 1M-cv mica polymorphs, the hkl reflections had similar intensities and very close positions being difficult to distinguish them especially for interstratificates of cv and tv layers. Tsipursky and Drits (1984) revealed semi-quantitatively the cv/tv proportions of several dioctahedral 2:1 phyllosilicates, finding a higher cv proportion in montmorillonites than in nontronites and beidellites. The cv polymorph shows a different reactivity to the tv in the dehydroxylation reaction. The cv/tv proportion can be estimated in illites and smectites by X-ray diffraction and thermal analysis (Drits et al. 1998). In smectites, the octahedral sheet tends to be cv, whereas illites have mainly a tv configuration (Cuadros, 2002); however, there is no linear relationship between the cv/tv ratio and smectite/illite proportion and some experimental discrepancies have been reported (Drits et al. 2006). For example, Tsipursky and Drits (1984) found that montmorillonite and Al-rich smectites are mainly cv, whereas McCarty and Reynolds (1995) discovered that the proportion of cv layers increased with tetrahedral Al content. Drits (2003) indicated that the cv/tv proportion is related with the formation mechanism of these phyllosilicates. Drits et al. (1998) proposed that illite-smectite interstratificates (I-S) formed from volcanic material contains a significant amount of cv layers, whereas I-S generated from weathered illitic material consists of tv 2:1 layers, according with investigations of smectite illitization of K-bentonites (Cuadros and Altaner, 1998), and hydrothermally altered rhyolitic volcanoclastic materials (Drits et al., 1996).

The wide diversity of compositions of these minerals is due to their capacity of isomorphous cation substitutions of Al^{3+} mainly by Fe^{3+} and Mg^{2+} in the octahedral sheets, and Si^{4+} by mainly Al^{3+} in the tetrahedral sheet. These cation substitutions produce compositional heterogeneity and order-disorder phenomena in the crystal

structure of these minerals that, along with the stacking ordering of the layers, existence of interstratificates of layers with different crystal-chemistry, and the small particle size of clays, make it difficult to obtain precise structural data by diffraction techniques. These cation substitutions can affect to the cv/tv proportion during the crystallization of these minerals. During the illitization process of montmorillonite, the formation of illite layers should lead to an increase of the proportion of tv layers. However, this process depends on the chemical composition and no proportional relationship between the polymorph ratio and the rate of transformation from smectite to illite has been found (Cuadros and Altaner, 1998; Drits 2003). Drits and Zviagina (2009) suggested that the cv/tv ratio can also depend on the octahedral cation arrangements.

On the other hand, the effect of cation substitutions on the tv forms of phyllosilicates has been studied by computational methods (Palin et al. 2004; Sainz-Díaz et al. 2001a, 2003a; Hernández-Laguna et al. 2006, Botella et al. 2004) showing that the cation ordering is highly dependent on the chemical composition. For smectite and illite there is not a long-range octahedral cation ordering but a short-range order in small domains (Sainz-Díaz et al. 2003a, 2003b). In tv, the $^{IV}Al^{3+}$ tends to be dispersed along the tetrahedral sheet. The octahedral Mg^{2+} and Fe^{3+} cations tend to be dispersed or clustered, respectively, along the octahedral sheet (Ortega-Castro et al. 2010). However, the cv polymorph has received less attention, and fewer studies related with cation substitution on cv forms have been reported (Sainz-Díaz et al. 2001b, 2005). The aim of this work is to study computationally the effect of the cation substitution arrangements (in tetrahedral and octahedral sheet) in the cis-vacant polymorph on the energy and geometrical parameters.

Computational methodology

In order to simulate different compositions of dioctahedral 2:1 phyllosilicates of the cv polymorphs, we used the SIESTA program (Soler et al., 2002) based on the Density Functional Theory (DFT), and numerical atomic orbitals (NAO). We used the Generalized Gradient Approximation with the PBE exchange correlation functional (Perdew, et al., 1996), and double-ζ polarized basis sets, exploring two *k* points in the Brilloin zone. To describe the core of atoms, we used norm-conserving pseudopotentials (Troullier and Martins, 1991). In each structure, we relax all atomic positions and lattice parameters using a force tolerance of 0.04 eV/Å. In samples with Fe, the minimum spin-state of Fe^{3+} cations was considered. The rest of calculation conditions have been optimized and described elsewhere (Sainz-Díaz et al. 2005). This methodology has been previously used satisfactorily reproducing the main crystallographic and spectroscopic properties of phyllosilicates (Sainz-Díaz et al. 2002; Botella et al. 2004; Hernández-Laguna et al. 2006). Powder X-ray diffraction (PXRD) pattern of the fully optimized cv and tv crystal structures were simulated by means of the Reflex program within the Material Studio package (Accelrys Inc.) for a average crystalline domain of 50 nm with a wavelength of 1.54 Å.

Models

The crystal structure and atomic positions were taken from the experimental data of models proposed by Tsipursky and Drits (1984) based on electron diffraction for the cv forms of dry samples of smectites and illites. The H atom coordinates were included manually and optimised previously by Sainz-Díaz et al. (2002). All samples are also completely dry in our simulations. The presence of additional water molecules would demand a higher computational effort and time, owing to the higher number of atoms and the appearance of several minima in a quite flat potential energy surface. This could

also produce a noise effect in our energy calculations between the cation arrangements of cv forms and between the cv and tv polymorphs.

We use one unit cell (40–43 atoms) with periodic boundary conditions. Hence, only formal cation substitutions can be included, that is, the minimum substitution degree is one cation per unit cell and no partial substitution was possible. This limitation generates models with cation contents that can be slightly different that in natural samples.

To study the effect of the cation substitutions in different layers we propose 16 models, based on the general formula $IC_{x+y}(Al_{4-x-z}Mg_xFe^{3+}_z)(Si_{8-y}Al_y)O_{20}(OH)_4$, shown in Table 1, in which the tetrahedral sheet Si^{4+} substitution by Al^{3+} and Al^{3+} by Mg^{2+} or Fe^{3+} in the octahedral sheet are considered. Several interlayer cations (IC) neutralize the layer charge coming from the isomorphic substitution: Na^+ (samples **cis1**, **cis3**, **cis5**, **cis7**, **cis10**, **cis13**, and **cis15**), K^+ (**cis2**, **cis4**, **cis6**, **cis8**, **cis11**, **cis14**, and **cis16**), and Ca^{2+} (**cis9** and **cis12**) are included. In this series, there are samples without tetrahedral charge (**cis3**, **cis4**, and **cis10-cis14**), samples with a certain tetrahedral charge, samples without octahedral charge (end member of beidellite, samples **cis1** and **cis2**), and samples with high octahedral charge (**cis10-cis12**). Samples with a high Fe content in the octahedral sheet are also included (**cis15** and **cis16**).

Samples **cis1** and **cis2** have only one tetrahedral sheet with substitution of one $^{IV}Al^{3+}$ per unit cell that is surrounded by other Si cations in the neighbour unit cell taking into account the periodical boundary conditions. Samples **cis3** and **cis4** have no tetrahedral substitution and one Mg^{2+} per unit cell in the octahedral sheet with only one interlayer cation per unit cell. Samples **cis5** and **cis6** have one $^{IV}Al^{3+}$ cation substitution per unit cell in only one tetrahedral sheet and the other tetrahedral sheet has no substitution. This sample has one Fe^{3+} cation per unit cell in the octahedral sheet and one interlayer cation

per unit cell. Samples **cis7** and **cis8** show one octahedral Mg^{2+} substitution and one tetrahedral $^{IV}Al^{3+}$ substitution with two ICs per unit cell and all tetrahedral cavities are occupied by IC's. **Cis9** is similar to this last one, with the same tetrahedral and octahedral composition but with one Ca^{2+} as IC per unit cell, where only half of the tetrahedral cavities are occupied with IC's. **Cis10** and **cis11** have no tetrahedral substitution and two Mg^{2+} cations per unit cell in the octahedral sheet with two interlayer cations per unit cell. **Cis12** is like this last one but with one Ca^{2+} as IC per unit cell. **Cis13** and **cis14** have no tetrahedral substitution and one Mg^{2+} and one Fe^{3+} cation per unit cell in the octahedral sheet with one IC per unit cell. **Cis15** and **cis16** show a high concentration of Fe^{3+} with two octahedral cations per unit cell and only one tetrahedral substitution, $^{IV}Al^{3+}$, in only one tetrahedral sheet, and one interlayer IC per unit cell (Table 1).

Charged samples have integer values of the charge per unit cell. Then these cation substitutions decrease the symmetry of the crystal structure, and different cation arrangements can exist for a certain cation composition. A specific crystallographic definition of the cation substitution sites should be established for the comparison of different cation arrangements. Considering a projection of these lattice structures on the plane (001), the tetrahedral Al^{3+} cation can be close to the (100) plane (T1) or close to the (200) plane (T2) (Fig. 1). Analogously the octahedral cation substitution can be close to the (100) plane (O1) or close to the (200) plane (O2) (Fig. 2). All our samples are in the T2 arrangement. We explore several cation substitution arrangements in order to determine the energy and geometrical differences. Similar arrangements have been studied previously by DFT methodology in trans-vacant polymorphs (Hernández-Laguna et al., 2006).

Results

In Table 2, the main crystal lattice parameters of the calculated structures with different cation arrangements for the monosubstituted (per unit cell in the tetrahedral or octahedral sheet) cv samples are compiled. The energy difference between cation-arrangements (relative energy from the minimum, ΔE = 0.0 eV) for each sample and the energy difference between the cv and tv forms are also included in Table 2. The same features are collected in Table 3 for the cv samples bisubstituted (per unit cell) in the octahedral sheet. The corresponding values of these features for the tv forms have been included in Tables 4 and 5 for comparisons (Hernández-Laguna et al. 2006).

Although the experimental studies of crystal lattice parameters were based on mixtures of tv and cv forms (Tsipursky and Drits, 1984), the calculated values of cell parameters are similar to the experimental values for clay minerals with similar compositions to our models in the cv (Tables 2 and 3) and tv samples (Tables 4 and 5). Nevertheless, the calculated values of the parameters *a* and *b* of cv and tv forms are slightly larger than the experimental values. No significant differences (< 2%) are observed in the calculated values of *a* within the series of cv samples. In general, samples with Mg have a slightly greater value of *a* (5.28-5.30 Å in **cis10**-**cis12**), and those with Fe has slightly smaller value of *a* (5.23 Å in **cis5** and **cis15**). Similar differences are observed in tv forms. The parameters *c* and β of the cv forms are smaller than in the tv forms (Tables 4 and 5), but these differences of *c* and β are balanced and the *d*(001) spacing ($c.\sin\beta$) is maintained at similar values for both forms, as it was expected from experimental values.

A linear relationship is found between the *d*(001) spacing ($c.\sin\beta$) and the ionic potential (IP = q/ir; q = formal charge, ir = ionic radius, Shannon 1976) of the interlayer cation (IC) for a series with the same composition and different IC. This linear regression is observed for samples with tetrahedral and octahedral charges,

214 $(Si_7Al)(Al_3Mg)(IC^{x+})_{2/x}$ (**cis7-cis9**) (Fig. 3a), and with only high octahedral charge,
215 $(Si_8)(Al_2Mg_2)(IC^{x+})_{2/x}$ (**cis10-cis12**) (Fig. 3b). This relationship indicates that with a
216 higher IP the IC will be smaller or with higher charge and it will interact more with the
217 tetrahedral cavity decreasing the *d*(001) spacing. For example, in samples with only one
218 tetrahedral substitution of Al^{3+} (^{IV}Al) per unit cell, **cis1** (IC = Na^+) shows a smaller
219 *d*(001) spacing (*c*.sinβ) than **cis2** (IC = K^+).

220 Small geometrical differences are observed between the cation arrangements. In
221 samples with only one octahedral substitution of Mg^{2+} per unit cell (**cis3** and **cis4**), three
222 possible relative positions of Mg^{2+} with respect to the IC can be considered: O1, where
223 the IC and Mg^{2+} are in the same (100) plane and in the same tetrahedral cavity (Fig. 2a);
224 O2a, where the IC is in the (100) plane and Mg^{2+} is in the (200) plane and both cations
225 are in the same (020) plane (Fig. 2b); and O2b, where the IC is in the (100) and (020)
226 planes and Mg^{2+} is in the (200) and (010) planes (Fig. 2c). In both samples, **cis3** and
227 **cis4**, the most stable distribution is the O1, owing to the proximity of IC and Mg^{2+} that
228 increases the electrostatic interactions between IC and the MgOHAl and apical MgOSi
229 oxygens that are highly charged due to the presence of Mg^{2+}. In **cis3** the least stable
230 cation arrangement is the O2a. In this case the IC and Mg^{2+} are also close and the
231 electrostatic interactions between IC and the O atoms joined to Mg^{2+} are also strong.
232 However the IC are between two Mg^{2+} cations in the same (020) plane with an IC…Mg
233 distance of 5.23 Å. This arrangement produces a higher distortion due to the higher size
234 of Mg^{2+} with respect to the Al^{3+} in octahedral coordination (Shannon 1976), increasing
235 slightly the value of the lattice parameter *a*. In **cis4** this O2a configuration is not so
236 unstable because this distortion is relaxed with a IC…Mg distance (6.00 Å) larger and a
237 higher lattice volume than in **cis3**. In the tv forms the relative energy of the cation
238 arrangements is the opposite, O2b is more stable than O1 (Table 4), although the energy

239 difference is very small. In general, the energy difference between these cation
240 arrangements is greater in the cv form than in tv (Sainz-Díaz et al., 2005). In the most
241 stable structure of **cis4**, the cv form is more stable than tv, probably due to that the
242 IC…Mg and HO…IC distances are slightly shorter in cv (5.16 and 3.81 Å) than in tv
243 (5.27 and 3.83 Å). In these samples, **cis3** and **cis4**, the configuration O1 has a higher
244 value of *b* because both IC and Mg^{2+} cations are in the same plane along the *b* axis
245 producing a slight distortion. The configuration O2b shows a high value of *d*(001)
246 spacing (*c*.sin*β*) with respect to the rest. On the other hand, these samples (**cis3** and **cis4**)
247 show smaller values of *d*(001) spacing than those with only tetrahedral charge, **cis1** and
248 **cis2** or **cis5** and **cis6**. This could possibly be caused by the octahedral source of negative
249 charges created by the isomorphic substitution of Mg^{2+}. This charge is more distributed
250 in the inner apical tetrahedral oxygens and attracts to the IC from both sides of the
251 interlayer space, whereas in **cis1** and **cis2** the charge defect comes from the external
252 basal tetrahedral sheet of only one side of the interlayer space. Similar effect was
253 detected in our calculated tv forms (Table 4). Sato et al. (1992) detected also
254 experimentally this effect in montmorillonite and beidellite with Na^+ and K^+ as IC.

255 In addition to the tetrahedral substitution, the octahedral substitution can be Fe^{3+}
256 instead of Mg^{2+} without generating octahedral charge (**cis5** and **cis6**). Keeping the
257 $^{IV}Al^{3+}$ substitution in the site T2 and the IC along the (100) plane, we can consider two
258 possible cation arrangements of Fe^{3+} with respect to the IC: O1, where the Fe^{3+} are
259 along the (100) plane; and O2 with the Fe^{3+} in (200) plane. No significant differences in
260 the lattice parameters values are observed between both cation arrangements (Table 2).
261 In both samples, O1 is slightly more stable than O2, like in **cis3** and **cis4**, but with
262 smaller energy differences. In these samples the tetrahedral Al substitution is only on
263 one part of the interlayer space producing an asymmetry in this space and the tetrahedral

charge makes that the IC are slightly displaced 0.1 Å from the center of interlayer to the tetrahedral sheet which support the Al substitution as in **cis1** and **cis2**. In the tv forms **trans5** and **trans6**, the O1 is also the most stable cation arrangement (Table 4).

Cation isomorphous substitutions can produce octahedral and tetrahedral charge simultaneously, with one Mg^{2+} cation in the octahedral sheet and one $^{IV}Al^{3+}$ in the tetrahedral sheet per unit cell. In this work we study this kind of substitution with different IC's, such as Na^{+}, K^{+}, and Ca^{2+}, in **cis7**, **cis8**, and **cis9**, respectively. Considering supercells of this series, all cation substitutions, $^{IV}Al^{3+}$ and Mg^{2+}, are disperse following the Lowenstein rule (Lowenstein, 1954) in the tetrahedral sheet and avoiding also $Mg^{2+}OMg^{2+}$ pairs in octahedral sheet. Taking into account the relative positions of $^{IV}Al^{3+}$ and Mg^{2+} each other and with respect to the IC, several possible cation arrangements can be considered. With divalent IC (**cis9**), only half of the tetrahedral cavities are occupied by IC. Considering that the $^{IV}Al^{3+}$ cations are in T2 position, the possible octahedral cation arrangements can be: O1, where the IC and Mg^{2+} are along the (100) plane (Fig. 2a); O2a, where the IC are along the (100) plane and the Mg^{2+} cations are in the planes (200) and (020) (Fig. 2b); and O2b, like the previous one but with the Mg^{2+} along the planes (200) and (010) (Fig. 2c). With monovalent IC (**cis7** and **cis8**) all tetrahedral cavities are occupied by IC. In all cases the O2b configuration is the most stable (Table 2), because both substitutions, $^{IV}Al^{3+}$ and Mg^{2+}, sources of the tetrahedral and octahedral charges, are more separate from each other than in the other configurations. In this series the energy differences between cation arrangements are much higher than in the above previous samples. Similar behaviour is observed in the tv forms of this series, **trans7**-**trans9**, where the O2b is the most stable cation arrangement (Table 4).

289 *Bisubstitutions in the octahedral sheet*

290 Instead of tetrahedral cation substitution, isomorphous substitutions of two Mg^{2+}
291 cations per unit cell can be produced. These substitutions generate octahedral charge
292 that is compensated by different IC's, Na^{+} (**cis10**), K^{+} (**cis11**), or Ca^{2+} (**cis12**). In
293 addition to the relative positions of the octahedral substitutions with respect to the IC,
294 we have to consider the specific cation arrangements among the octahedral cations. As
295 explained elsewhere (Sainz-Díaz et al., 2002; Hernández-Laguna et al., 2006), three
296 kinds of arrangements can be considered: *ortho*, where the cation substitution sites are
297 the nearest neighbors to a distance of 2.9-3.1 Å; *meta*, where these substituted sites are
298 separated by one Al^{3+} with an inter-site distance about 5 Å; and *para*, when these sites
299 are separated by two Al^{3+} (with an inter-site distance close to 6 Å) in the same unit cell,
300 respectively. Taking into account the translational crystal lattice periodicity and the
301 neighbor unit-cells, these cation arrangements considered in one unit cell will be related
302 with more arrangements. Then, two *ortho* arrangements can exist, one forming a chain
303 of Mg^{2+} along the *a* axis direction (Fig. 4a), and another one that is the same of the *para*
304 distribution where all patterns, *ortho*, *meta* and *para*, co-exist (Fig. 4b). Besides, the
305 *meta* distribution has also two more Mg^{2+} cations as second neighbors within a *meta*
306 ordering pattern with the vicinal cells (Fig. 4c and 4d).

307 In all cases the *meta* arrangement is the most stable and the *ortho* is the least
308 stable with higher energy differences than in the above previous arrangements (Table
309 3). In the samples with monovalent IC, **cis10** and **cis11**, two possible *meta* distributions
310 can exist: *meta*-1, where IC and Mg^{2+} are in the same (020) plane (Fig. 4d), and *meta*-2
311 (Fig. 4c). This last one is slightly more stable than the *meta*-1. In all cases, no
312 significant difference in the crystal lattice parameters is found within the cation
313 arrangements. This is consistent with previous results on tv forms (Table 5) indicating

the tendency of Mg^{2+} to be dispersed along the octahedral sheet of phyllosilicates (Cuadros et al. 1999, Sainz-Diaz et al. 2000, Hernández-Laguna et al. 2006). The energy differences derived of the cation distribution along of the octahedral sheet are greater than those derived from IC/tetrahedral and IC/octahedral cation arrangements in previous samples. The *ortho* configuration has the highest polyhedron distortions and the highest repulsive interactions of the negative charge generated by the presence of two $^{VI}Mg^{2+}$ cations as first neighbors separated by 2.98 Å, which forms a chain of Mg^{2+} cations along the *a* axis direction. This arrangement produces a high concentration of charge along this direction and a high distortion in the coupling of polyhedra due to the higher ionic radius of Mg^{2+} than Al^{3+}. Therefore, the probability to find a MgMg pair will be very low in these samples. In the *para* configuration this distortion is partial and this configuration has lower energy than *ortho* and higher energy than *meta*.

A semiquantitative approach to analyze the energetic of the cation arrangement in this Al_2Mg_2 system is to consider the interaction energies between both cations as first, and second neighbours in the *ortho*, *meta* and *para* arrangements in one unit cell. These interactions can be defined as cation exchange potential terms (J_{AA}^{i}) in the octahedral sheet described elsewhere (Sainz-Díaz et al. 2003a): Specific formulae neglecting third and fourth neighbour interactions were applied to the tv forms previously (Hernández-Laguna et al. 2006). Then, the J_{AA}^{1} and J_{AA}^{2} were determined from the energy differences of *ortho*, *meta* and *para* arrangements in the unit cell. J_{AA}^{1} and J_{AA}^{2} mean the energy change for forming two homocationic pairs ($Al^{3+}\cdot\cdot Al^{3+}$ and $Mg^{2+}\cdot\cdot Mg$) from two heterocationic pairs (2 $Al^{3+}\cdot\cdot Mg^{2+}$) at first and second neighbourhood ($J_{AA}^{i} = E_{AA}^{i} + E_{BB}^{i} - 2E_{AB}^{i}$), respectively (Table 6). Exchange potentials at first neighbours, J_{AA}^{1}, are approximately seven times larger than the second neighbour terms owing to the shorter distances between cations in the octahedral sheet.

The J_{AA}^1 values in the cv polymorphs are 1.5 and 1.75 times larger than in tv for Na^+ and K^+ samples, respectively, whereas J_{AA}^2 values in cv are 2.8, and 12.9 times larger than in tv for Na^+ and K^+ samples, respectively. This could indicate qualitatively that the octahedral Mg^{2+} cations in cv forms tend to be more dispersed than in tv forms. On the other hand, in Ca^{2+} samples both exchange potentials in cv are similar that those in tv (Hernandez-Laguna et al 2006). Plotting both exchange potentials for cv forms as a function of the formal charge/ionic radius of the IC (Fig. 5) a non-linear decreasing is observed, showing an opposite trend with respect to the tv samples (Hernandez-Laguna et al, 2006). The interaction of the IC with the octahedral cation exchange dynamics is clearly observed in both cv and tv polymorph, but the opposite trend is surprising. The position of the OH's around the vacant is quantitatively different for the cation exchange in the octahedral sheet and the effect of the IC on this cation exchange is different in both cv and tv polymorphs. Nevertheless, this study is based only in exchange potentials for first and second neighbours, however our results highlight the necessity of further work on cation ordering in cv forms with larger models.

The double substitution in the octahedral sheet can be also by one Mg^{2+} and Fe^{3+} per unit cell without tetrahedral substitution, generating less interlayer charge, **cis13** (IC = Na^+) and **cis14** (IC = K^+). In all cases the *meta* configurations are the most stable, whereas the *ortho* and *para* have similar energy each other (Table 3). In this series (Mg^{2+}/Fe^{3+}) the energy difference between *meta* and *ortho* configurations is smaller than in the previous **cis10**-**cis12** series. The Fe^{3+} cation does not generate a negative charge in the layer, then the repulsive interactions are smaller and the charge distribution is more dispersed than in the series with two Mg^{2+} cations. No significant difference in the crystal lattice parameters are observed between the cation arrangements. In the tv forms **trans13** and **trans14** (Table 5) the *meta* configuration is

364 also the most stable cation arrangement and the *ortho* one is the least stable one.
365 However, in tv forms the *para* one has similar energy to *meta* one (Hernández-Laguna
366 et al. 2006).
367
368 The double octahedral substitution can be with two Fe^{3+} cations and one
369 tetrahedral $^{IV}Al^{3+}$ substitution within one unit cell, **cis15** (IC = Na^{+}) and **cis16** (IC = K^{+}).
370 In this series there is no octahedral charge and the interlayer charge comes from the
371 tetrahedral sheet. Considering the $^{IV}Al^{3+}$ site in T2 and the IC in the (100) plane, we
372 calculate the *ortho*, *meta*, and *para* arrangements of Fe^{3+} cations. In all cases of this
373 series, the *ortho* configuration is the most stable and the *meta* one is the least stable
374 (Table 3). This is consistent with previous experimental and theoretical results on tv
375 forms indicating the tendency of Fe^{3+} to be clustered along the octahedral sheet of
376 phyllosilicates (Cuadros et al. 1999; Sainz-Diaz et al. 2000; Hernández-Laguna et al.
377 2006). However, in the cv forms, the energy differences between these configurations
378 are greater than in tv forms (Table 5).
379
380 *Cis-vacant / trans-vacant configurations*
381 The cv/tv proportion in these phyllosilicates can be determined with the
382 parameter ε (ε = |*c*.cos β |/*a*) (Drits and McCarty 1996). This can be calculated from the
383 *d* values obtained from the indexing of the reflection lines in powder XRD. In the
384 quantitative determination of cv/tv proportions, values of ε for pure cv and pure tv
385 structures must be determined previously. However, different experimental values have
386 been reported for similar samples, such as ε_{cis} = 0.308 and ε_{trans} = 0.383 (McCarty and
387 Reynolds 1995), and ε_{cis} = 0.300-0.302 and ε_{trans} = 0.400 (Drits and McCarty 1996),
388 being a handicap to apply it to other samples. We can calculate this parameter from a

theoretical crystal structure with one specific cation content, a cation distribution for only cv or tv forms and for different cation compositions and cation arrangements (Tables 2-5). In our samples, we observe a significant variation of this parameter with the nature of cation substitution and also with the relative arrangements of these substituted cations, being in the range of 0.23 – 0.35 for cv forms. Nevertheless, the average value for all cv samples is 0.294 that is consistent with the experimental value (0.300-0.302) obtained by Drits and McCarty (1996) with natural samples, where a mixture of all situations, local cation compositions and cation arrangements, can exist. Excluding the less probable cation arrangements (structures with high energy, relative energy > 0.5 eV) the average value of ε is 0.297, closer to the experimentally estimated value. There is no clear relationship between the nature of cation substitution and the variation of ε. Nevertheless, samples with Ca^{2+} as IC (**cis9** and **cis12**) show higher values of ε than those with K^{+} or Na^{+}. Samples with high content of Fe^{3+} (**cis15** and **cis16**) show also high values of ε. The variation of ε due to the cation arrangement some times is greater than that due to the nature of cation substitution.

We can observe clearly the different values of ε in tv forms that appears in the range of 0.38-0.43. In general, the calculated *c* values are slightly greater than those estimated experimentally. In the tv forms, like in cv, no clear relationship between Δε and nature of cation substitution and cation arrangement was found. In general, samples with Mg^{2+} show lower ε.

In general the energy difference between cv and tv forms ($\Delta E_{cv\text{-}tv}$) is smaller than that between the cation arrangements (Tables 2 and 3). The $\Delta E_{cv\text{-}tv}$ can vary with the cation arrangement according to experimental results (Drits et al. 2006). The pattern of the relative cation distribution can be different in cv and tv forms. In some cases we compare the energy differences between those cv and tv configurations with similar

414 relative cation arrangement. When the cation arrangements have similar energy, we
415 compare average energy values of each polymorph. In cases where the energy
416 differences between cation arrangements are important (> 0.2-0.25 eV), we used the
417 most stable configuration for each polymorph for energy comparisons. Values
418 calculated with different criteria are shown when the cv/tv energy difference changes
419 with the comparison criterion (Tables 2 and 3). In samples with only a tetrahedral
420 substitution (**cis1** and **cis2**) the energy difference between polymorphs are negligible.
421 With the additional presence of Fe in octahedral sheet (**cis5**, **cis6**, **cis15**, and **cis16**), the
422 cv forms are more stable than tv. Samples with one octahedral Mg cation per unit cell
423 (**cis3**, **cis4**, **cis7**-**cis9**, and **cis13**-**cis14**) show that the tv are slightly more stable than cv.
424 The energy difference depends on the criterion for the cation arrangement comparison
425 and average values were considered when the energy difference between cation
426 arrangements are lower than 0.1 eV and only the most stable ones were considered for
427 the rest of cases (for example, the O1 arrangements of **cis7** and **cis8** were not considered
428 due to their high energy and consequently low probability to appear). In samples with
429 two octahedral Mg^{2+} cation substitutions and no tetrahedral charge (**cis10**-**cis12**) the
430 configuration cv is slightly more stable than tv.
431
432 We simulated the PXRD patterns of our models based on their crystal lattice
433 structures and atomic positions. This simulation can be useful to experimental work in
434 order to predict or identify reflections observed in the laboratory or to introduce this
435 information in the simulated annealing programs used for identifying different crystal
436 phases in a clay mineral. In all cv and tv forms of our series, the 060 reflection appears
437 at 1.51-1.52 Å (1.53 Å in **cis11**) (61.1-60.7 2θ units) that is characteristic of
438 dioctahedral phyllosilicates (beidellite and illite, Brindley and Brown 1980) and it can

439 be used for distinguishing the trioctahedral phyllosilicates where this 060 reflection
440 appears at 1.53 – 1.55 Å (60.5-59.5 2θ units).

441 Comparing different cation arrangements for the same chemical composition,
442 the reflections positions are almost the same, changing only the relative intensities of
443 some reflections. For example in bisubstituted series in octahedral sheet, the PXRD
444 patterns of *ortho* and *para* arrangements are very similar (for **cis13**, Fig. 6a and 6b),
445 whereas the *meta* form shows more differences in the relative intensities, especially the
446 020 reflection that is more intense in *meta* (Fig. 6c) than in *ortho* and *para*, probably
447 due to the differences in the cell lattice parameter *b* (Table 3) that produces a
448 superposition of the 020, $1\,\bar{1}\,0$, and 110 reflections increasing the intensity of this peak.
449 This effect is more clear in **cis10** (with 2 Mg^{2+} per unit cell), where the 020, or (020 +
450 $1\,\bar{1}\,0$ + 110) reflections are more intense than the 001 one (Fig. 7a). This variation of
451 relative intensities of XRD reflections with the octahedral cation distribution was
452 previously detected experimentally by Drits and Zviagina (2009). In general the high
453 intensity of the peak at 19.4-19.8º is mainly due to the 110 reflection in the cv forms or
454 to the 020 reflection in the tv forms. In **cis10** the 110, $02\,\bar{2}$, 111, and $11\,\bar{3}$ reflections are
455 more intense (Fig. 7a) than in tv where the 020, $1\,\bar{1}\,1$, $11\,\bar{2}$, and 112 reflections (Fig. 7b)
456 are significantly more intense than in cv. With respect to the peak positions, the main
457 differences are observed in the $11\,\bar{2}$, 112, $11\,\bar{3}$, and 202 reflections that appear at 25.2º,
458 28.2º, 31.8º, and 41.1º in **cis10** (Fig.7a) and at 24.4º, 29.3, 31.0º, and 43.0º in **trans10**,
459 respectively (Fig. 7b).

460 In **cis15** the most intense reflection is the 001 one (Fig. 8a), being the relative
461 intensities of the other reflections much lower than in the previous samples.
462 Nevertheless, the relative intensities of the rest of peaks are similar, except the 002,
463 $11\,\bar{3}$, and 060 reflections that are much less intense than in **cis10**. Similar differences

were found in the tv forms (Fig. 8b). In this sample, the $01\bar{1}$ reflection appears at 13.3º, like in **cis13,** but it is not detected in **cis10**. In **trans15** the *ortho*, *meta* and *para* arrangements show similar positions of reflections with slight differences in relative intensities in some reflections. However, some differences in the relative intensities and reflection positions can be observed between the cv and tv forms of the most stable cation arrangement, like in **cis10**/**trans10** samples described above. These differences between cv and tv forms are similar for all samples and are consistent with that found experimentally by Drits (2003), and Zviagina et al. (2007).

Discussion

In general the cv forms can present similar cation arrangements that the tv forms. Within a certain chemical composition, the most stable cation arrangements are similar for both polymorphs observing some differences in the relative energies between arrangements. Nevertheless, the energy differences related with cation arrangements are greater than those between cv and tv polymorphs. These energy differences between cv and tv forms are too small to explain the probability to crystallize a cv or tv form with relation to the chemical composition. Hence other factors can affect the cv and tv formation in clay minerals and no prediction can be performed about the direct effect of cation substitution on the cv/tv proportion. Though the temperature effect has not been taken into account in our calculations, we can infer that the formation of these polymorphs in the nucleation is not controlled thermodynamically. The different proportion of these polymorphs in natural samples and conditions will be controlled by kinetic conditions during the nucleation of these minerals. This fact can explain the non-linear relationship between illite/smectite and tv/cv proportions found experimentally in natural samples (Drits, 2003; Drits and Zviagina, 2009).

The presence of water in the interlayer space in our models would generate more realistic models, but it would require a high computational cost. Besides, these more complex models would introduce another variable in our research moving over of our main aim, which is focused in the relative energy between the cation arrangements of cv forms and between the cv/tv forms. Within a systematic research, the scope of this work is to observe this behavior in dry samples. This work opens a window to explore more variables, such as, the water effect on these energy differences, in further researches.

Nevertheless, the presence of water will be in the interlayer space and interacting with the IC and water could alter only slightly the relative proportion of these polymorphs, because the energy differences are very small and lower than that from cation arrangements. However, the water effect will be very important during the nucleation process and formation of these polymorphs, where higher amount of water can be present in hydrothermal or quasi-amorphous-phases scenarios that are out of the scope of this work. From our relative energy results with ideal samples, layers with high Mg content and no tetrahedral Al tend to be in a cv form, however during a illitization process the tetrahedral Al content increases and the Mg content can decrease and the tv form will be more stable and the system will tend to nucleate a tv form.

A remarkable consideration should be explained in order to understand the cv/tv formation and the discrepancies found. We suggest that the crucial moment is the nucleation step of each layer. The probability of formation of cv or tv polymorphs will depend on the chemical composition of the local environment of this crystal-nucleus and the nucleation kinetics. However, one layer cannot support cv and tv forms simultaneously. This means that the crystal growth of the nucleated layer will maintain the initial structure of the polymorph nucleated (cv or tv). The attachment of the aggregation units during this crystal growth will depend more on the chemical

514 composition of the local environment than on the type of polymorph, due to the low
515 energy differences between cv and tv forms. This can explain that natural samples with
516 the same chemical composition can appear with different cv/tv polymorphism.

517 Besides, the cation arrangement is also important thermodynamically, even more
518 than the cv/tv proportion because of the higher energy differences between cation
519 arrangements. Hence both phenomena, local cation arrangement and cv/tv
520 polymorphism, can be established during the nucleation step. However, it is more
521 probable that the cv/tv forms are nucleated initially and after the cation arrangements
522 are established during the crystal growth, depending on the local chemical environment.

523 Another possibility is the possible formation of amorphous pre-nuclei phases
524 where the cv/tv polymorphs can be pre-established. The atoms in these amorphous
525 phases will have a higher mobility and some cation arrangements could be formed
526 during the equilibration time just before the nucleation looking for a low energy state.
527 This hypothesis would be within the recent concept of polyamorphism that have been
528 found in carbonates (Cartwright et al. 2012), where different amorphous phases can
529 exist and induce the nucleation of the corresponding crystal polymorph. In our minerals,
530 two different amorphous phases could be related with cv and tv crystal forms. However,
531 this subject is out of the scope of the present work and further investigations will be
532 necessary to understand the nucleation process of phyllosilicates.

533

534 The cation exchange potentials indicate a greater dispersion tendency of octahedral Mg
535 cations in the cv forms than in tv. Nevertheless, in our calculations no temperature
536 effect has been included. Hence our energy calculations cannot predict the possible
537 preferences for cation arrangements that can occur during the cv/tv transformation in the
538 dehydroxylation of cv forms where migrations of octahedral cations are produced at

539 high temperatures for generating tv forms and the cation arrangements could be altered
540 in the short-range ordering of octahedral cations.

541 There are differences in intensities and positions in some reflections of the
542 PXRD patterns between cv and tv forms, however these differences can change with the
543 chemical composition and the cation arrangement. This fact is observed in our ideal
544 theoretical models, but it should be taken into account in the experimental patterns with
545 mixture of layers with different cation arrangements. Hence our calculated models can
546 be useful for the experimental work in crystal structure determinations in
547 phyllosilicates.

548

549 **ACKNOWLEDGEMENTS**

550 Authors are thankful to the "Centro Técnico de Informática" of CSIC, "Centro
551 de Supercomputación de Galicia" (CESGA) and the "Centro de Supercomputación de la
552 Universidad de Granada" for allowing the use of its computational facilities; and to J.
553 Cuadros for his useful reviewing work. E. Escamilla-Roa is thankful to Agencia
554 Española de Cooperación Internacional (AECI) for financial support. This work was
555 supported by Spanish Ministerio de Educación y Ciencia (MEC) and European FEDER
556 grants BTE2002-03838, FIS2010-22322-C02-02, CGL2005-02681 and CGL208-02850
557 grants.

558

559 **REFERENCES CITED**

560 Bernal, J.D. (1949) The Physical Basis of live. Proceedings of the Physical Society A,
561 62, 537-558.
562
563 Botella, V., Timón, V., Escamilla-Roa, E., Hernández-Languna, A., and Sainz-Díaz,
564 C.I. (2004) Hydrogen bonding and vibrational properties of hydroxy groups in the
565 crystal lattice of dioctahedral clay minerals by means of first principles calculations.
566 Physics and Chemistry of Minerals, 31, 475-486.
567

Cartwright, J.H.E., Checa, A.G., Gale, J.D., Gebauer, D., and Sainz-Díaz, C.I. (2012) Calcium Carbonate Polyamorphism and Its Role in Biomineralisation: How many ACCs are there?. Angewandte Chemie International Edition (in press).

Cuadros J. (2002) Structural insights from the study of Cs-exchanged smectites submitted to wetting-and-drying cycles. Clay Minerals, 37, 473-486.

Cuadros, J., and Altaner, S.P. (1998) Characterization of mixed-layer illite-smectite from bentonites using microscopic, chemical, and X-ray methods; constraints on the smectite-to-illite transformation mechanism. American Mineralogist, 83, 762-774.

Cuadros, J., Sainz-Díaz, C.I., Ramírez, R., and Hernández-Laguna, A. (1999) Analysis of Fe segregation in the octahedral sheet of bentonitic illite-smectite by means of FTIR, 27 Al MAS NMR and reverse Monte Carlo simulations. American Journal of Science, 299, 289-308.

Drits, V.A. (2003) Structural and chemical heterogeneity of layer silicates and clay minerals. Clay Minerals, 38, 403-432.

Drits, V.A., Salyn, A.L. and Sucha, V. (1996) Structural transformations of interstratified illite-smectites from Dolna Ves hydrothermal deposits: dynamics and mechanisms. Clays and Clay Minerals, 44, 181-190.

Drits, V.A., Lindgreen, H., Salyn, A.L., Ylagan, R., and McCarty, D.K. (1998) Semiquantitative determination of trans-vacant and cis-vacant 2:1 layers in illites and illite-smectites by thermal analysis and X-ray diffraction. American Mineralogist, 83, 1188-1198.

Drits, V.A., and McCarty, D.K. (1996) The nature of diffraction effects from illite and illite-smectite consisting of interstratified trans-vacant and cis-vacant 2:1 layers; a semiquantitative technique for determination of layer-type content. American Mineralogist, 81, 852-863.

Drits, V.A., McCarty, D.K., and Zviagina, B.B. (2006) Crystal-chemical factors responsible for the distribution of octahedral cations over trans- and cis-sites in dioctahedral 2:1 layer silicates. Clays and Clay Minerals, 54, 131-152.

Drits, V.A., and Zviagina, B.B. (2009) Trans-vacant and cis-vacant 2:1 layer silicates: structural features, identification, and occurrence. Clays and Clay Minerals, 57, 405-415.

Drits, V.A., Plançon A., Sakharov, B.A., Besson, G., Tsipursky, S.I., and Tchoubar, C. (1984) Diffraction effects calculated for structural models of K-saturated montmorillonite containing different types of defects. Clay Minerals, 19, 541-562.

Herd, C.D.K., Blinova, A., Simkus, D.N., Huang, Y., Tarozo, R., Alexander, C.M.O.D., Gyngard, F., Nittler, L.R., Cody, G.D., Fogel, M.L., Kebukawa, Y., Kilcoyne, A.L.D., Hilts, R.W., Slater, G.F., Glavin, D.P., Dworkin, J.P., Callahan, M.P., Elsila, J.E., De Gregorio, B.T., and Stroud, R.M. (2011) Origin and Evolution of Prebiotic Organic Matter As Inferred from the Tagish Lake Meteorite. Science, 332, 1304-1307.

Hernández-Laguna, A., Escamilla-Roa, E., Timón, V., Dove, M.T., and Sainz-Díaz, C.I. (2006) DFT study of the cation arrangements in the octahedral and tetrahedral sheets of dioctahedral 2:1 phyllosilicates. Physics and Chemistry of Minerals, 33, 655-666.

Hibbitts, C.A., and Szanyi, J. (2007) Physisorption of CO_2 on non-ice materials relevant to icy satellites. Icarus, 191, 371-380.

Lebofsky, L.A., Feierberg, M.A., and Tokunaga, A.T. (1982) Infrared observations of the dark side of Iapetus. Icarus, 49, 382-386.

Lowenstein, W. (1954) The distribution of aluminium in the tetrahedra of silicates and aluminates. American Mineralogist 39, 92-96.

McCarty, D.K., and Reynolds, R.C. (1995) Rotationally disordered illite/smectite in Paleozoic K-bentonites. Clays and Clay Minerals, 43, 271-284.

Méring, J., and Oberlin, A. (1971). Smectites. In: The Electron-Optical Investigation of Clays (J.A.Card, ed.). 193-229. Mineralogical Society, London, UK.

Mustard, J.F., Murchie, S.L., Pelkey, S.M., Ehlmann, B.L., Milliken, R.E., Grant, J.A., Bibring, J.P., Poulet, F., Bishop, J., Dobrea, E.N., Roach, L., Seelos, F., Arvidson, R.E., Wiseman, S., Green, R., Hash, C., Humm, D., Malaret, E., McGovern, J.A., Seelos, K., Clancy, T., Clark, R., Marais, D.D., Izenberg, N., Knudson, A., Langevin, Y., Martin, T., McGuire, P., Morris, R., Robinson, M., Roush, T., Smith, M., Swayze, G., Taylor, H., Titus, T., and Wolff, M. (2008) Hydrated silicate minerals on Mars observed by the Mars Reconnaissance Orbiter CRISM instrument. Nature, 454, 305-309.

Ortega-Castro, J., Hernandez-Haro, N., Dove, M.T., Hernández-Laguna, A., and Sainz-Díaz, C.I. (2010) Density functional theory and Monte Carlo study of octahedral cation ordering of Al/Fe/Mg cations in dioctahedral 2:1 phyllosilicates. American Mineralogist, 95, 209-220.

Palin, E.J., Dove, M.T., Hernández-Laguna, A., and Sainz-Díaz, C.I. (2004) A computational investigation of the Al/Fe/Mg order-disorder behavior in the dioctahedral sheet of phyllosilicates. American Mineralogist, 89, 164-175.

Perdew, J.P., Burke, K., and Ernzerhof, M. (1996) Generalized Gradient Approximation Made Simple. Physical Review Letters, 77, 3865-3868.

Rubin, A.E. (1997) Mineralogy of meteorite groups. Meteoritics and Planetary Science, 32, 231-247.

Sainz-Díaz, C.I., Hernández-Laguna, A., and Dove, M.T. (2001a) Modelling of dioctahedral 2:1 phyllosilicates by means of transferable empirical potentials. Physics and Chemistry of Minerals, 28, 130-141.

Sainz-Díaz, C.I., Hernández-Laguna, A., and Dove, M.T. (2001b) Theoretical modelling of cis-vacant and trans-vacant configurations in the octahedral sheet of illites and smectites. Physics and Chemistry of Minerals, 28, 322-331.

Sainz-Díaz, C.I., Palin, E.J., Hernández-Laguna, A., and Dove, M.T. (2003a) Octahedral cation ordering of illite and smectite. Theoretical exchange potential determination and Monte Carlo simulations. Physics and Chemistry of Minerals, 30, 382-392.

Sainz-Díaz, C.I., Palin, E.J., Hernández-Laguna, A., and Dove, M.T. (2003b) Monte Carlo simulations of ordering of Al, Fe, and Mg cations in the octahedral sheet of smectites and illites. American Mineralogist, 88, 1033-1045.

Sainz-Díaz, C.I., Timón, V., Botella, V., Artacho, E., and Hernández-Laguna, A. (2002) Quantum mechanical calculations of dioctahedral 2:1 phyllosilicates: Effect of octahedral cation distributions in pyrophyllite, illite, and smectite. American Mineralogist, 87, 958-965.

Sainz-Díaz, C.I., Escamilla-Roa, E., and Hernández-Laguna, A. (2005) Quantum mechanical calculations of trans-vacant and cis-vacant polymorphism in dioctahedral 2:1 phyllosilicates. American Mineralogist, 90, 1827-1834.

Sato, T., Watanabe, T., and Otsuka, R. (1992) Effects of layer charge, charge location, and energy change on expansion properties of dioctahedral smectites. Clays and Clay Minerals, 40, 103-113.

Shannon, R.D. (1976) Revised effective ionic radii and systematic studies of interatomic distances in halides and chalcogenides. Acta Crystallographica A32, 751-767.

Soler, J. M., Artacho, E., Gale, J. D., García, A., Junquera, J., Ordejón, P., and Sánchez-Portal, D. (2002) The SIESTA method for ab-initio order-N materials simulation. Journal of Physics: Condensed Matter, 14, 2745-2779.

Swadling, J. B., Coveney, P. V., and Greenwell, H. C. (2010) Clay minerals mediate folding and regioselective interactions of RNA: A large-scale atomistic simulation study. Journal of the American Chemical Society, 132, 13750–13764.

Troullier, N., and Martins, J.L. (1991) Efficient pseudopotentials for plane-wave calculations. Physical Review B, 43, 1993-2006.

Tsipursky, S.I., and Drits, V.A. (1984) The distribution of octahedral cations in the 2:1 layers of dioctahedral smectites studied by oblique-texture electron diffraction. Clay Minerals, 19, 177-193.

Zviagina, B.B., Sakharov, B.A., and Drits, V.A. (2007) X-ray diffraction criteria for the identification of trans- and cis-vacant varieties of dioctahedral micas. Clays and Clay Minerals, 55, 467–480.

Captions of Figures

Figure 1.- Crystal structure of cis-vacant (a) and trans-vacant (b) forms of dioctahedral 2:1 phyllosilicates. The unit cell used in the calculations is marked with a square. The octahedral sheet is represented by polyhedra in pink colour, and the H, IC, O and Si atoms are described in black, grey, red, and yellow colours, respectively. The hexagons that are formed by tetrahedral and octahedral cations are marked by dashed and plain lines, respectively. Vertical dashed lines represent the (100) and (200) planes.

Figure 2.- Cation arrangements for simultaneous monosubstitutions in tetrahedral and octahedral sheet: O1 (a), O2a (b), O2b (c). The H, IC, octahedral substitution, and tetrahedral substituted atoms are represented as balls. The octahedral substitutions are in green colour. The H, IC, O, Al and Si atoms are in black, grey, red, pink, and yellow colours, respectively.

Figure 3.- Relationship between ionic potential of IC and averaged $c\sin\beta$ values for the most stable cation arrangements of samples with substitution of $^{IV}Al^{3+}$ and Mg^{2+} (a), and samples with bisubstitution of Mg^{2+} (b).

Figure 4.- The *ortho* (a), *para* (b), *meta*2 (c), and *meta*1 (d) cation arrangements of the samples bisubstituted in the octahedral sheet. The H, IC, and octahedral substitution are highlighted as balls. The octahedral substitutions are in blue colour. The H, IC, O, Al and Si atoms are in black, grey, red, pink, and yellow colours, respectively. In part d, the black line represents the [020] plane.

Figure 5.- Cation exchange potentials (in eV) at first and second neighbours as a function of the formal charge/ ionic radius (in formal-charge/Å).

Figure 6.- Powder X-ray diffraction (PXRD) patterns simulated for the fully optimized crystal structures of cv sample **cis13** in the *ortho* (a), *para* (b), and *meta* (c) octahedral cation arrangements.

Figure 7.- PXRD patterns simulated for *meta* arrangement of **cis10** (a) and **trans10** (b) forms.

Figure 8.- PXRD patterns of **cis15** (a) and **trans15** (b) forms of in the most stable cation arrangement.

Table 1.- Chemical composition of the samples studied in the cis-vacant form. Structural formulae on the basis O_{20} $(OH)_4$ (T = tetrahedral, Oc = octahedral)

Sample	Si^{4+} (T)	Al^{3+} (T)	Al^{3+} (Oc)	Mg^{2+} (Oc)	Fe^{3+} (Oc)	Interlayer cation
cis1	7	1	4			Na^+
cis2	7	1	4			K^+
cis3	8		3	1		Na^+
cis4	8		3	1		K^+
cis5	7	1	3		1	Na^+
cis6	7	1	3		1	K^+
cis7	7	1	3	1		$2Na^+$
cis8	7	1	3	1		$2K^+$
cis9	7	1	3	1		Ca^{2+}
cis10	8		2	2		$2Na^+$
cis11	8		2	2		$2K^+$
cis12	8		2	2		Ca^{2+}
cis13	8		2	1	1	Na^+
cis14	8		2	1	1	K^+
cis15	7	1	2		2	Na^+
cis16	7	1	2		2	K^+

762 Table 2.- Relative energy (in eV) and main crystal lattice parameters (distances in Å,
763 angles in degrees) of the cation arrangements calculated and experimental values
764 (Tsipursky and Drits, 1984) of monosubstituted samples for cv polymorphs.

sample	ΔE*	a	b	c	β	$c\sin\beta$	ε	$\Delta E_{cis\text{-}trans}$†
Exp		5.20	9.01	10.0-10.2	99.5	9.85-9.91	0.300-0.302	
Cis1		5.25	9.08	9.99	98.9	9.87	0.294	-0.002
Cis2		5.26	9.11	10.10	98.7	9.98	0.290	-0.008
Cis3 O1	0.0	5.26	9.15	9.86	97.1	9.78	0.232	0.025‡
Cis3 O2a	0.063	5.28	9.09	9.88	99.0	9.76	0.293	0.064§
Cis3 O2b	0.042	5.27	9.11	9.92	97.7	9.83	0.252	0.075‡
Cis4 O1	0.0	5.28	9.17	9.92	98.3	9.82	0.271	-0.024‡
Cis4 O2a	0.010	5.30	9.13	9.95	99.2	9.82	0.300	0.016§
Cis4 O2b	0.072	5.28	9.14	10.01	97.9	9.91	0.261	0.073‡
Cis5 O1	0.0	5.23	9.08	9.93	98.9	9.81	0.294	-0.011§#
Cis5 O2	0.010	5.23	9.08	9.95	99.5	9.82	0.314	
Cis6 O1	0.0	5.25	9.11	10.06	98.8	9.94	0.293	-0.015‡
Cis6 O2	0.010	5.25	9.11	10.10	99.1	9.97	0.304	
Cis7 O2b	0.0	5.25	9.10	10.04	97.9	9.95	0.263	0.025#
Cis7 O2a	0.272	5.27	9.09	10.00	99.0	9.88	0.297	
cis7 O1	0.505	5.25	9.11	10.02	99.1	9.89	0.302	0.204‡
Cis8 O2b	0.0	5.28	9.16	10.14	97.8	10.05	0.261	0.024#
Cis8 O2a	0.295	5.30	9.15	10.14	99.0	10.02	0.299	
Cis8 O1	0.533	5.27	9.18	10.16	98.1	10.02	0.272	0.222‡
Cis9 O2b	0.0	5.29	9.08	9.95	100.4	9.79	0.340	0.097#
Cis9 O2a	0.294	5.32	9.06	9.93	101.7	9.72	0.379	
Cis9 O1	0.335	5.28	9.13	9.92	100.6	9.75	0.346	0.041‡

765 * Relative energy of the cation arrangements for each sample (relative energy from the minimum, ΔE =
766 0.0 eV). The standard deviations are lower than $2x10^{-4}$ eV. † Energy difference between the cv and tv
767 polymorphs, $\Delta E = E_{cis} - E_{trans}$. The energy values are negative, then negative values of ΔE mean that the
768 cv form is more stable than tv. ‡ Forms with similar relative positions of cations. § Energy difference
769 taken from average energy values of each polymorph. # Difference between the most stable cation-
770 arrangement of each polymorph.
771

Table 3.- Relative energy (in eV) and main lattice parameters (distances in Å, angles in degrees) of the cation arrangements of cv polymorphs calculated for octahedrally bisubstituted samples (o, m, and p, mean *ortho*, *meta* and *para*, respectively) and experimental crystallographic values (Tsipursky and Drits 1984).

sample	ΔE*	a	b	c	β	$c\sin\beta$	ε	$\Delta E_{cis\text{-}trans}$†
Exp		5.20	9.01	10.0-10.2	99.5	9.85	0.300-0.302	
Cis10m2	0.0	5.25	9.11	9.97	99.2	9.84	0.304	-0.063‡
Cis10m1	0.045	5.28	9.05	9.98	99.5	9.84	0.312	
Cis10p	0.232	5.27	9.09	9.98	98.5	9.87	0.280	
Cis10o	0.741	5.27	9.08	9.97	98.2	9.87	0.270	
Cis11m2	0.0	5.28	9.19	10.01	97.4	9.93	0.244	-0.033‡
Cis11m1	0.053	5.30	9.12	10.03	99.9	9.88	0.325	
Cis11p	0.218	5.29	9.15	10.04	98.6	9.93	0.284	
Cis11o	0.779	5.29	9.13	10.0	98.2	9.90	0.270	
Cis12m	0.0	5.31	9.06	9.91	100.8	9.73	0.350	-0.004
Cis12p	0.185	5.30	9.10	9.88	99.5	9.74	0.308	
Cis12o	0.644	5.29	9.10	9.81	98.0	9.72	0.258	
Cis13m	0.0	5.26	9.11	9.86	97.9	9.77	0.233	0.059‡
Cis13o	0.146	5.27	9.09	9.87	99.0	9.75	0.293	
Cis13p	0.186	5.27	9.09	9.85	99.1	9.73	0.296	
Cis14m	0.0	5.28	9.14	9.92	99.1	9.80	0.285	0.032‡
Cis14p	0.176	5.29	9.13	9.92	99.9	9.78	0.322	
Cis14o	0.190	5.28	9.14	9.92	99.9	9.77	0.323	
Cis15o	0.0	5.23	9.09	9.92	99.4	9.79	0.310	-0.193
Cis15p	0.308	5.22	9.04	9.91	99.1	9.79	0.300	
Cis15m	0.390	5.23	9.05	9.93	99.3	9.80	0.307	
Cis16o	0.0	5.25	9.16	10.00	99.4	9.87	0.311	-0.223
Cis16p	0.347	5.25	9.10	10.01	99.2	9.88	0.305	
Cis16m	0.438	5.25	9.09	10.00	99.1	9.87	0.301	

* Relative energy of the cation arrangements for each sample (relative energy from the minimum, ΔE = 0.0 eV). The standard deviations are lower than 2×10^{-4} eV. †Energy difference between the most stable cation arrangements for cv and tv polymorphs, $\Delta E = E_{cis} - E_{trans}$. The energy values are negative, then negative values of ΔE mean that the cv form is more stable than tv. The errors are lower than 2×10^{-4} eV. ‡Difference between polymorphs with similar arrangements of cations.

785 **Table 4.-** Lattice parameters (distances in Å, angles in degrees) of the tv polymorphs of
786 the monosubstituted samples and relative energy of the cation arrangements calculated
787 and experimental values (Tsipursky and Drits 1984).
788

sample	ΔE*	a	b	c	β	$c\sin\beta$	ε
exp		5.18	9.01	10.05-10.2	101.4	9.8-9.99	0.383†, 0.400‡
trans1		5.26	9.00	10.05	101.9	9.83	0.394
Trans2		5.29	9.12	10.12	102.1	9.90	0.401
Trans3 O2	0.0	5.27	9.12	10.07	103.0	9.81	0.430
Trans3 O1	0.008	5.28	9.13	10.16	105.3	9.80	0.508
Trans4 O2	0.0	5.29	9.16	10.08	102.5	9.84	0.412
Trans4 O1	0.026	5.30	9.16	10.06	102.3	9.83	0.404
Trans5 O1	0.0	5.25	9.05	10.07	102.9	9.82	0.428
Trans5 O2	0.061	5.25	9.05	10.05	102.5	9.81	0.414
Trans6 O1	0.0	5.27	9.07	10.19	102.8	9.94	0.428
Trans6 O2	0.045	5.27	9.08	10.18	102.7	9.93	0.425
Trans7 O2b	0.0	5.26	9.12	10.10	101.8	9.89	0.393
Trans7 O1	0.325	5.27	9.13	10.11	102.0	9.89	0.399
trans7 O2a	0.342	5.25	9.13	10.10	101.8	9.89	0.393
Trans8 O2b	0.0	5.29	9.17	10.23	102.1	10.00	0.405
Trans8 O1	0.336	5.29	9.17	10.21	102.1	9.98	0.405
Trans8 O2a	0.352	5.29	9.17	10.21	102.1	9.98	0.405
Trans9 O2b	0.0	5.29	9.10	10.02	102.6	9.78	0.413
Trans9 O2	0.356	5.29	9.10	10.03	102.7	9.78	0.417
Trans9 O1	0.391	5.30	9.09	10.07	103.8	9.78	0.453

789 * Relative energy of the cation arrangements for each sample (relative energy from the
790 minimum, ΔE = 0.0 eV). The standard deviations are lower than $2x10^{-4}$ eV. †
791 Experimental values from McCarty and Reynolds (1995). ‡ From Drits and McCarty
792 (1996).
793
794
795
796
797
798

Table 5.- Lattice parameters (distances in Å, angles in degrees) and relative energy (eV) of the cation arrangements calculated for tv samples octahedrally bisubstituted (o, m, and p, mean *ortho*, *meta* and *para*, respectively) and experimental values (Tsipursky and Drits 1984).

sample	ΔE*	*a*	*b*	*c*	β	*c*sinβ	ε
exp		5.18	9.01	10.05-10.2	101.4	9.8-9.99	0.383†, 0.400‡
Trans10m	0.0	5.26	9.10	9.99	101.6	9.79	0.382
Trans10p	0.230	5.25	9.12	10.06	101.9	9.84	0.395
Trans10o	0.568	5.26	9.10	9.98	101.6	9.78	0.382
Trans11m	0.0	5.28	9.15	10.07	101.8	9.86	0.390
Trans11p	0.291	5.30	9.15	10.08	101.5	9.88	0.379
Trans11o	0.610	5.27	9.15	10.08	101.6	9.87	0.385
Trans12m	0.0	5.29	9.11	9.95	103.1	9.69	0.426
Trans12p	0.142	5.28	9.09	10.02	104.2	9.71	0.466
Trans12o	0.618	5.27	9.11	9.96	102.4	9.73	0.406
Trans13m	0.0	5.26	9.08	10.01	102.6	9.77	0.415
Trans13p	0.008	5.27	9.08	10.05	103.3	9.78	0.439
Trans13o	0.365	5.26	9.09	10.0	102.9	9.75	0.424
Trans14m	0.0	5.29	9.14	10.05	102.7	9.80	0.418
Trans14p	0.036	5.29	9.12	10.08	103.0	9.82	0.429
Trans14o	0.311	5.28	9.15	10.03	102.5	9.79	0.411
Trans15o	0.0	5.25	9.01	10.06	103.5	9.78	0.447
Trans15p	0.119	5.25	9.03	10.03	102.3	9.80	0.407
Trans15m	0.220	5.24	9.02	10.02	102.2	9.79	0.404
Trans16o	0.0	5.27	9.08	10.11	102.6	9.87	0.418
Trans16p	0.110	5.27	9.07	10.16	102.1	9.93	0.404
Trans16m	0.232	5.27	9.06	10.13	102.5	9.89	0.416

* Relative energy of the cation arrangements for each sample (relative energy from the minimum, ΔE = 0.0 eV). The standard deviations are lower than $2x10^{-4}$ eV. †Experimental values from McCarty and Reynolds (1995). ‡ From Drits and McCarty (1996).

811
812 **Table 6**.- Exchange potentials (eV) of octahedral cations for cv $Si_8Al_2Mg_2$ samples at
813 first and second neighbours.
814

Sample	J_{AA}^1	J_{AA}^2
Cis10 (IC=Na^+)	0.509	0.075
Cis11 (IC=K^+)	0.561	0.092
Cis12 (IC=Ca^{2+})	0.459	0.068

815
816

Figures

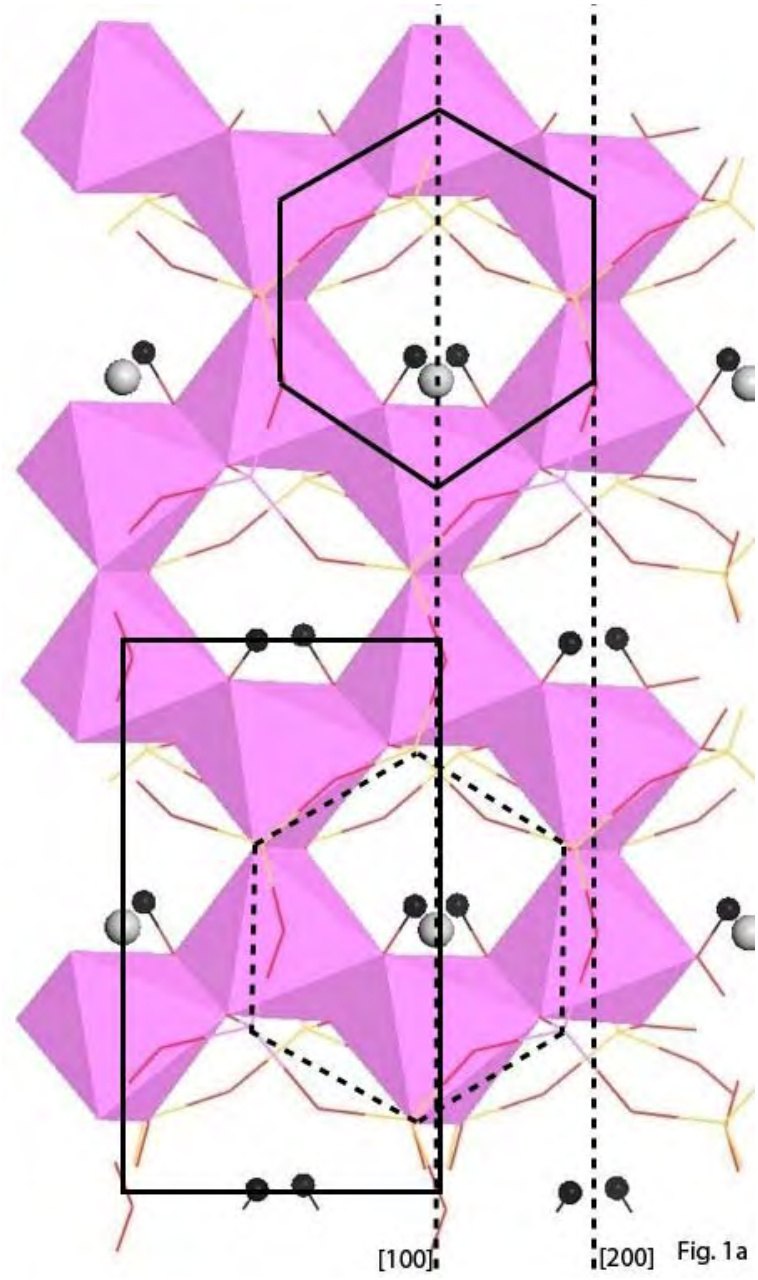

Fig. 1a

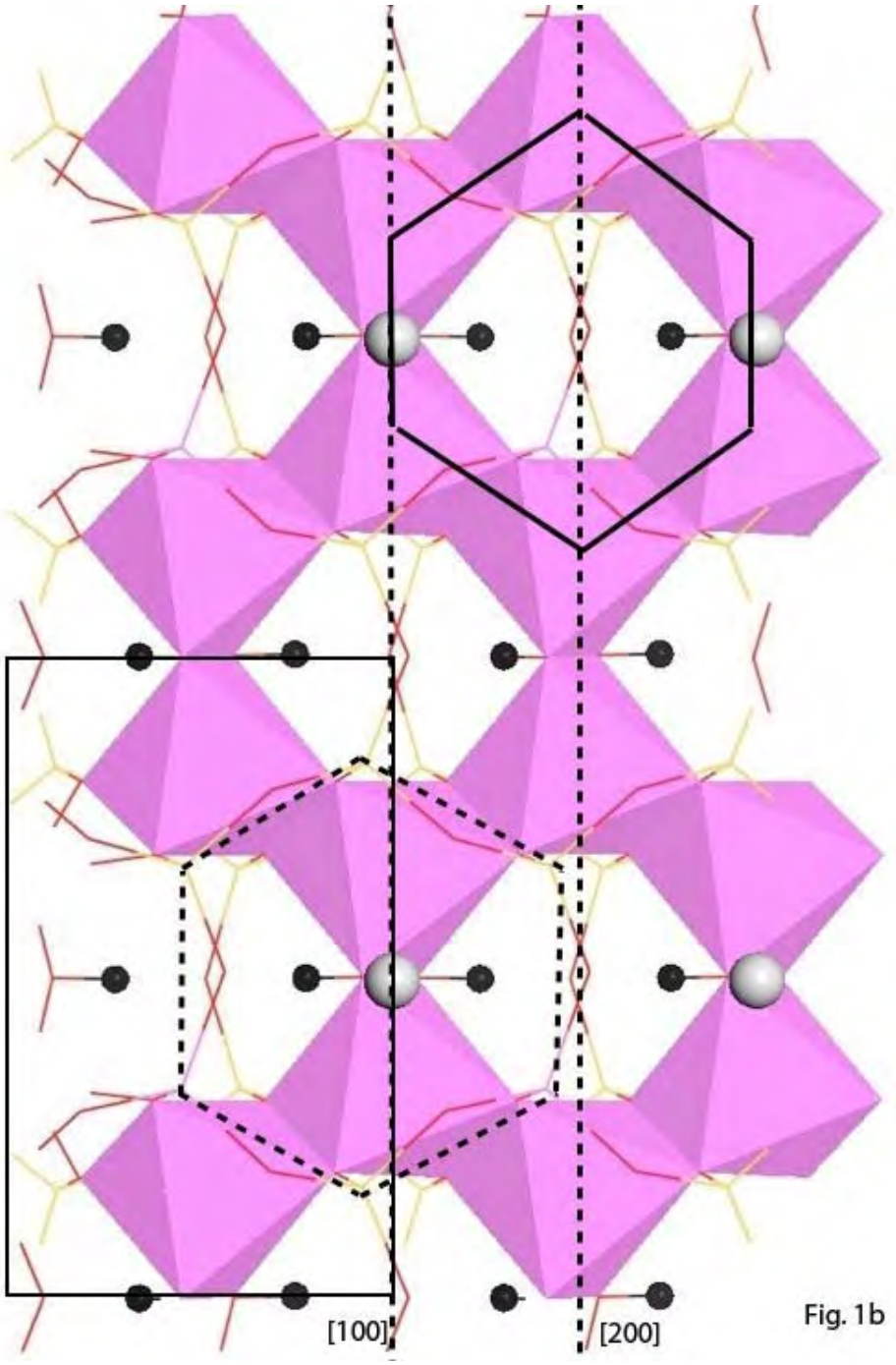

Fig. 1b

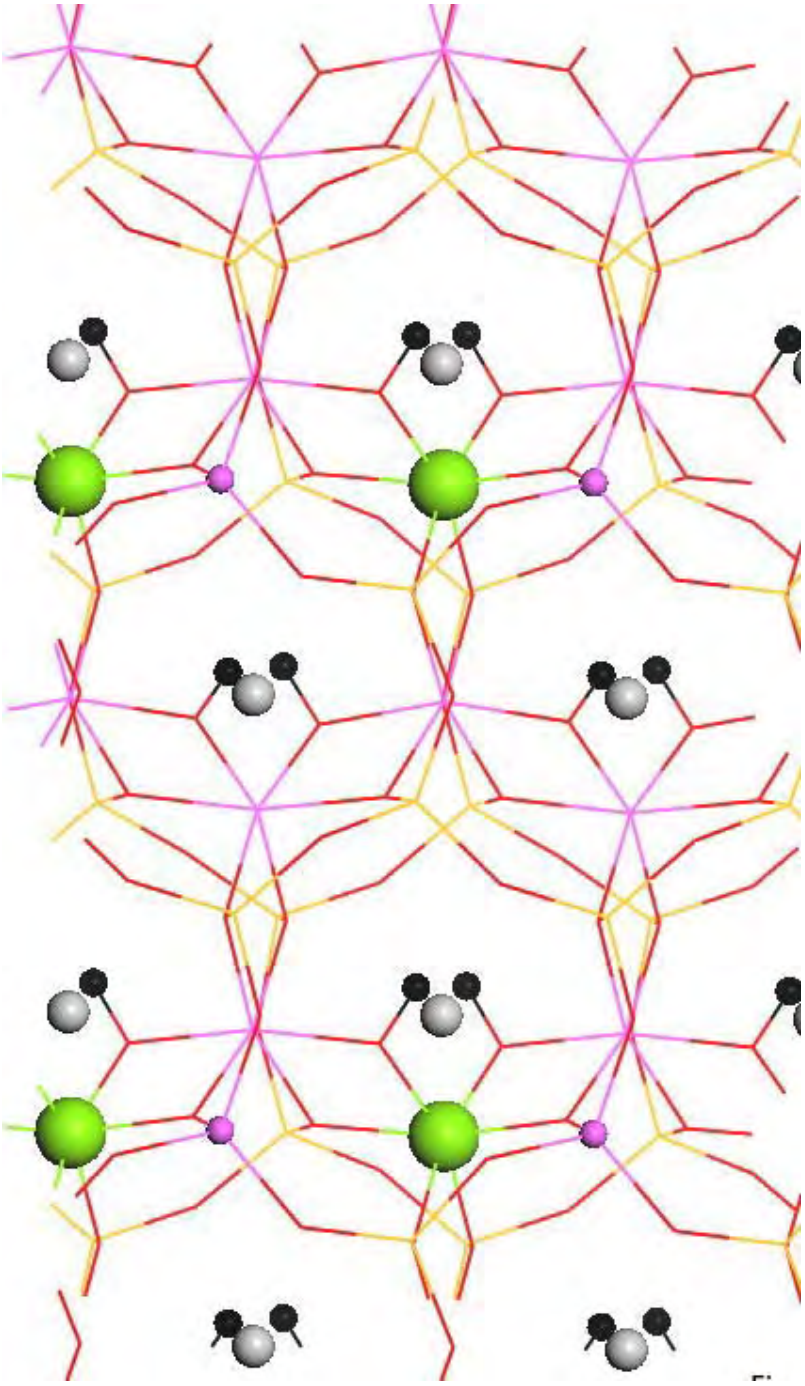

Fig. 2a

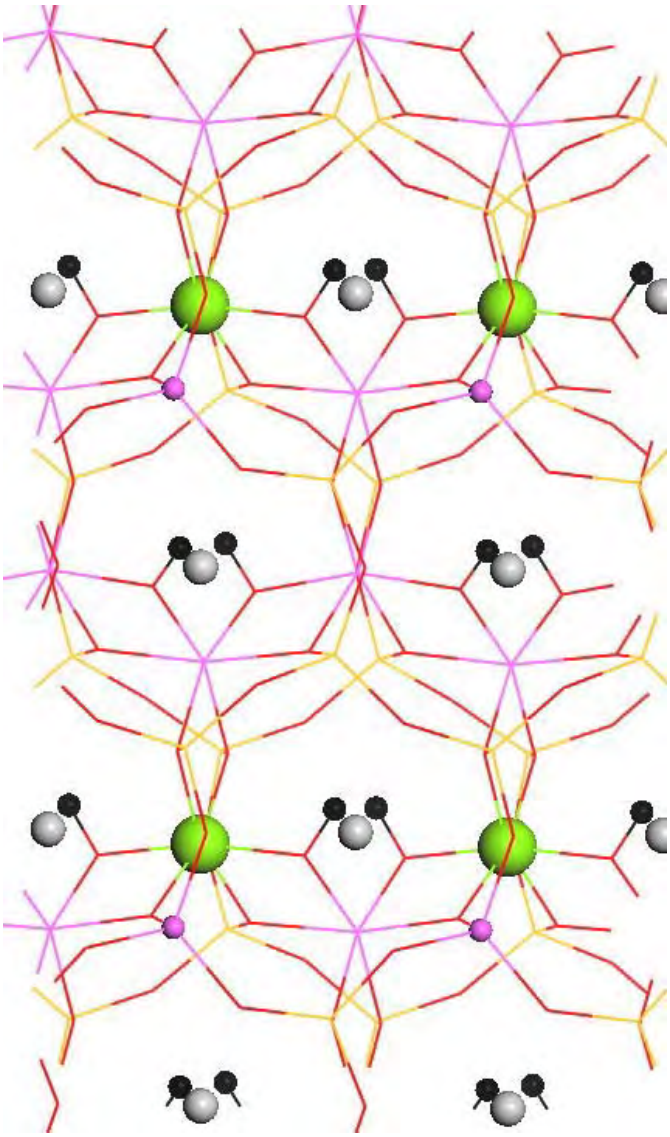

fig 2b

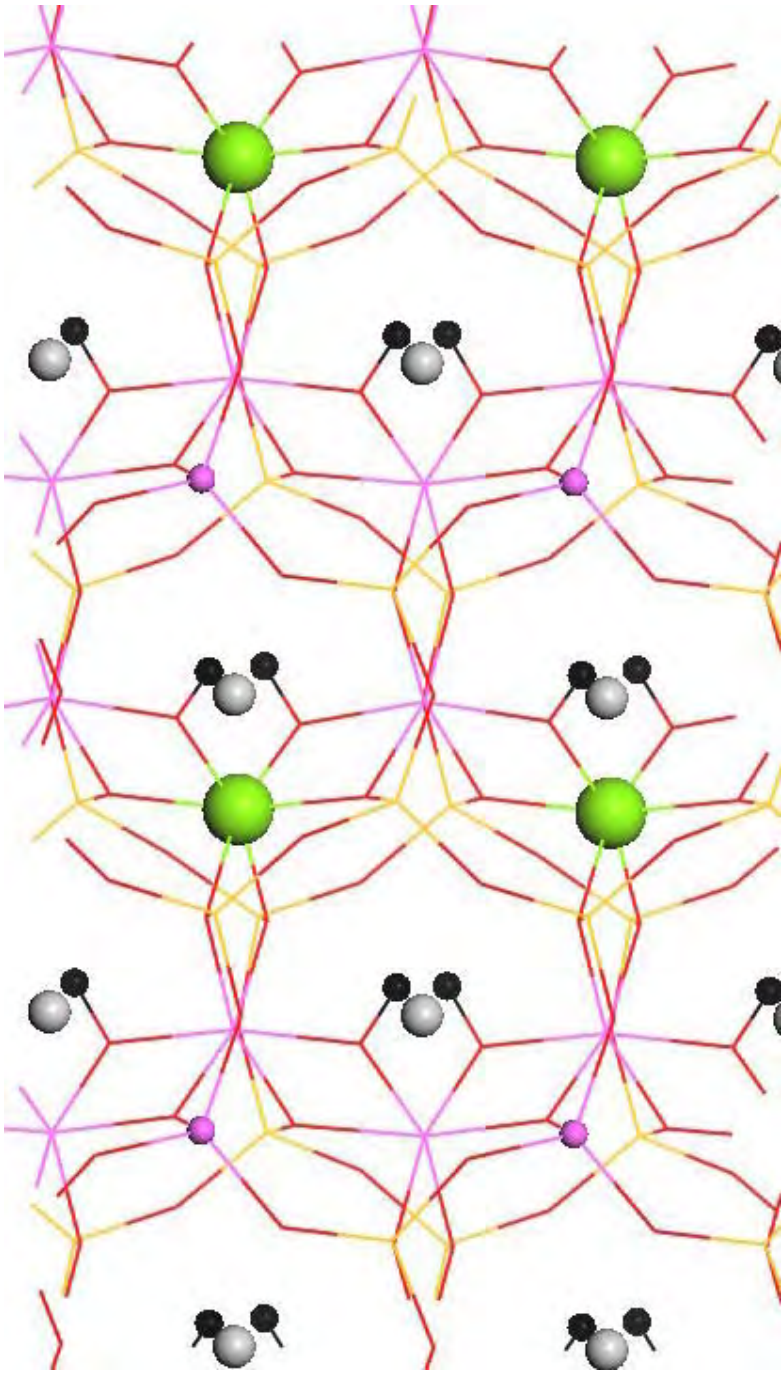

Fig. 2c

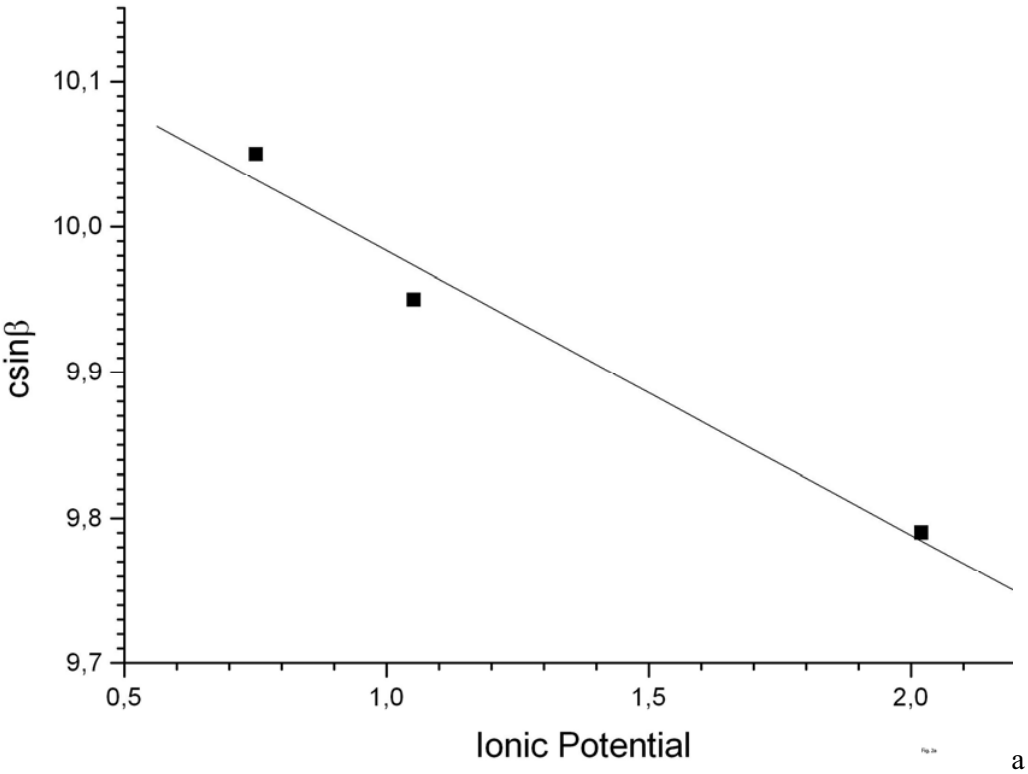
10,1
10,0
9,9
9,8
9,7
csinβ
0,5
1,0
1,5
2,0
Ionic Potential

a

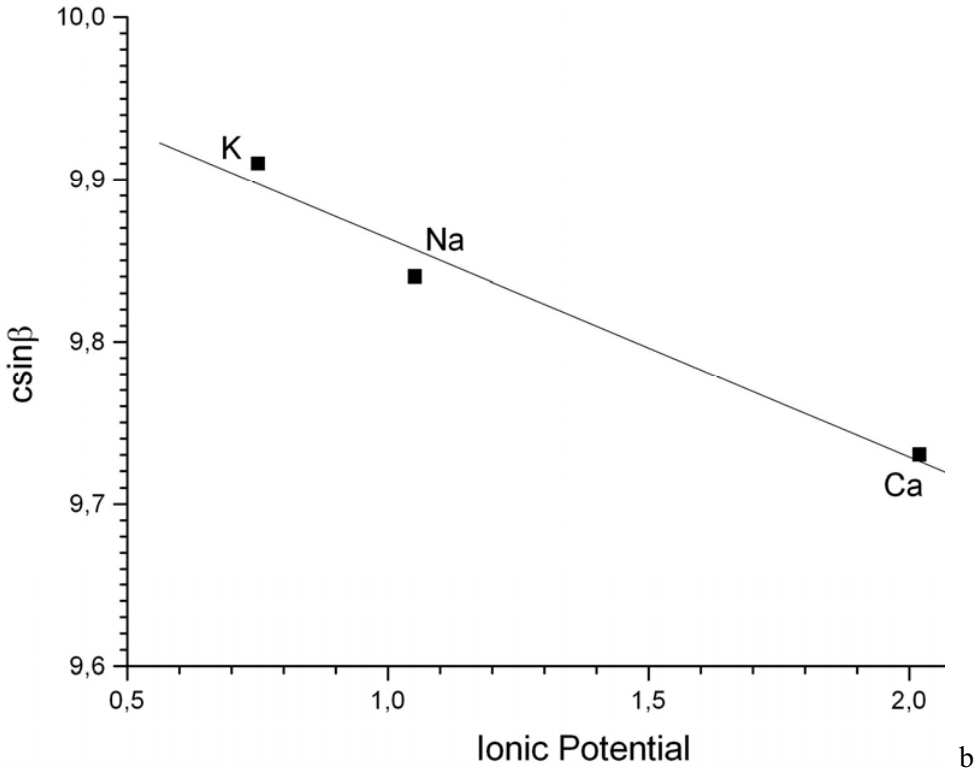
10,0
9,9
9,8
9,7
9,6
csinβ
K
Na
Ca
0,5
1,0
1,5
2,0
Ionic Potential

b

Fig 3

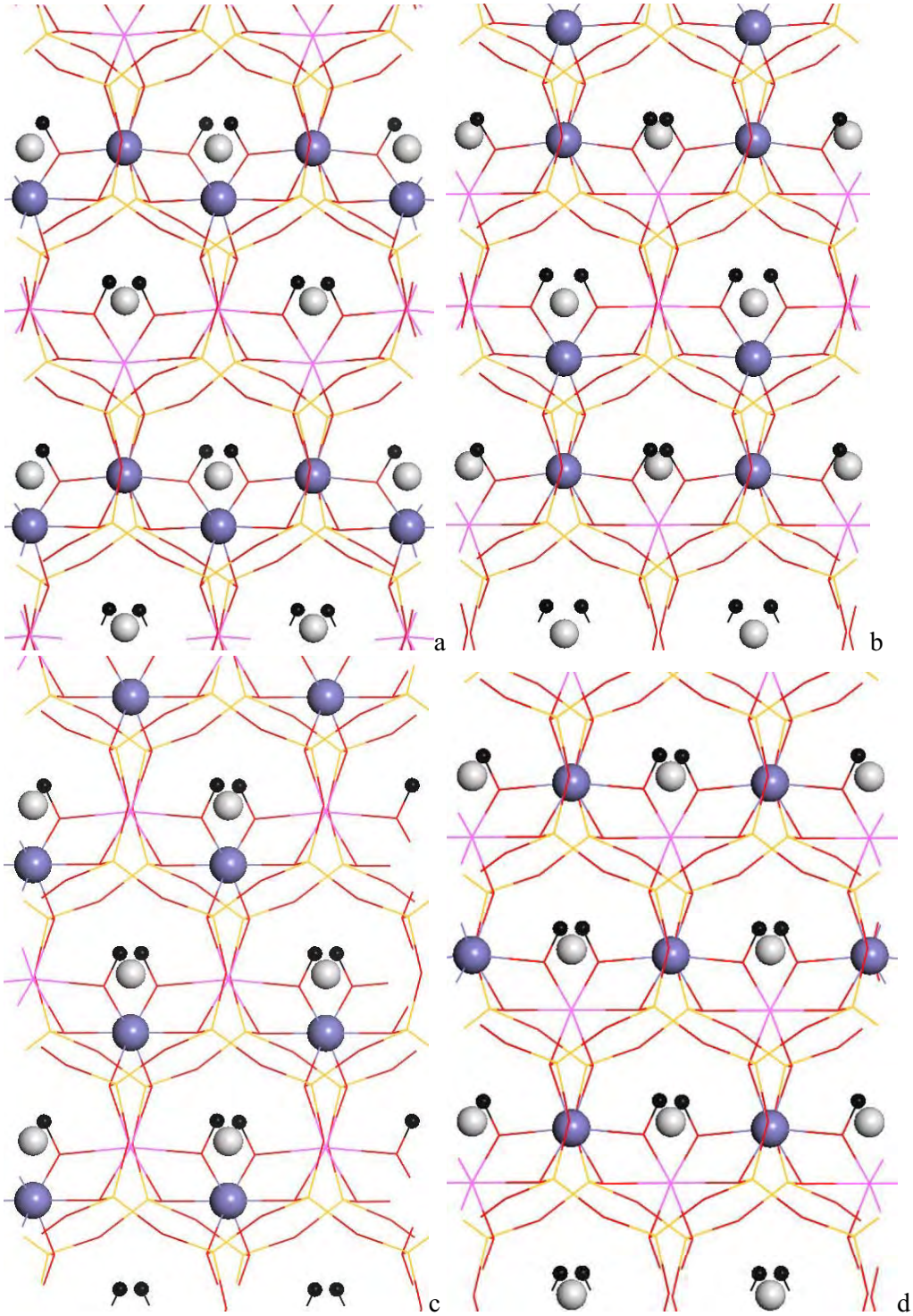

Fig. 4

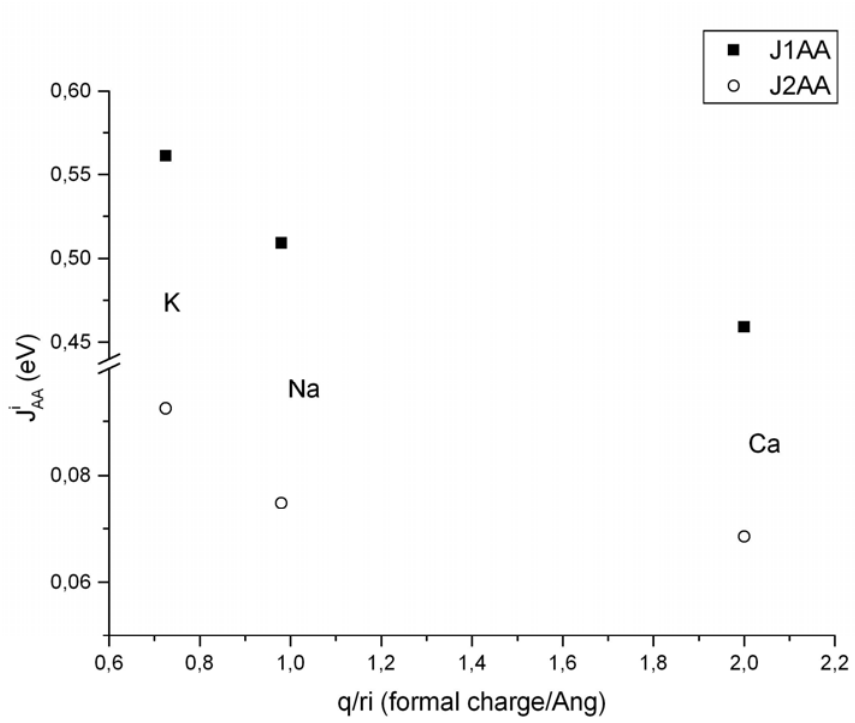
J1AA
J2AA
0,60
0,55
0,50
0,45
0,08
0,06
K
Na
Ca
J^i_{AA} (eV)
0,6
0,8
1,0
1,2
1,4
1,6
1,8
2,0
2,2
q/ri (formal charge/Ang)

Fig. 5

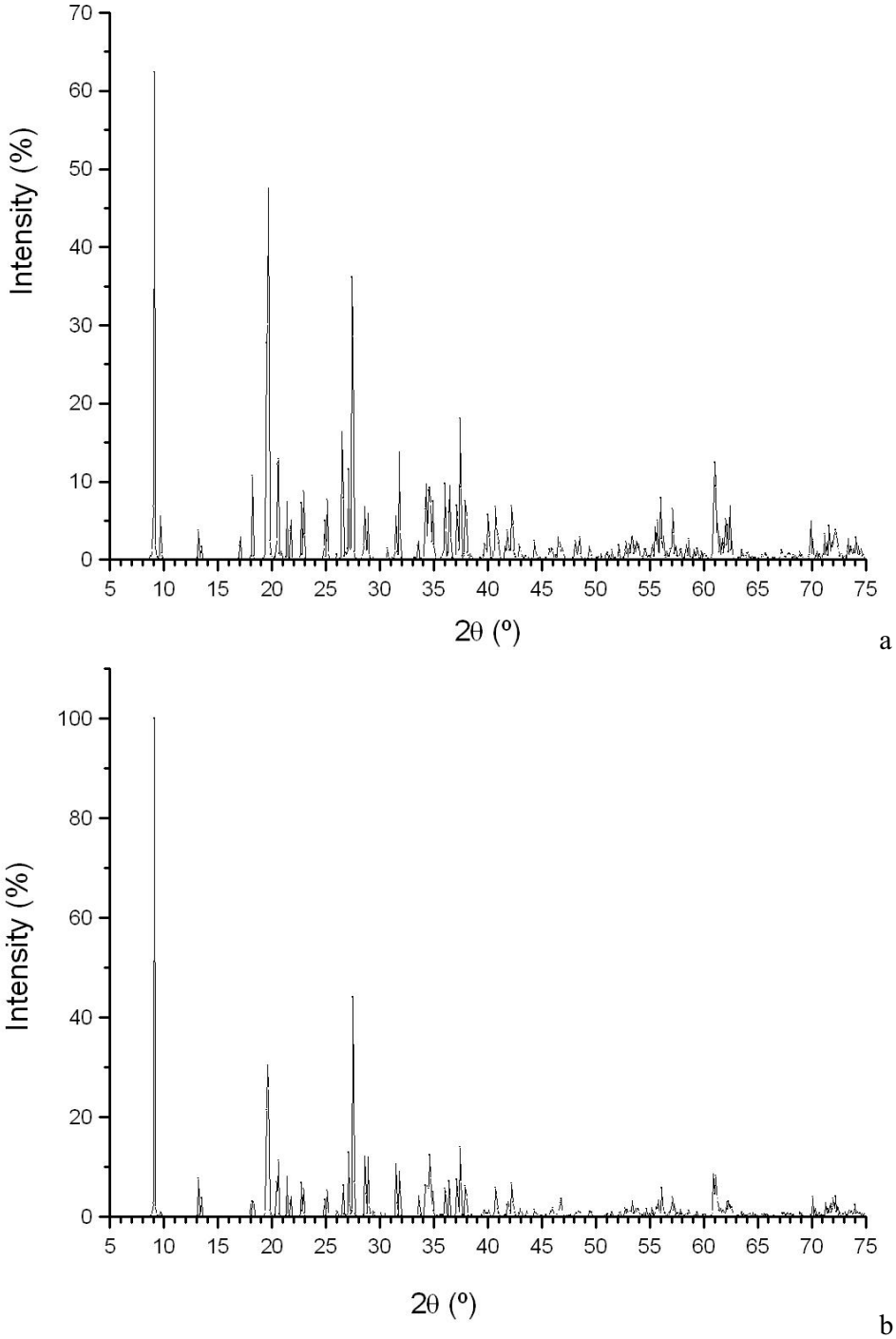

Fig. 6

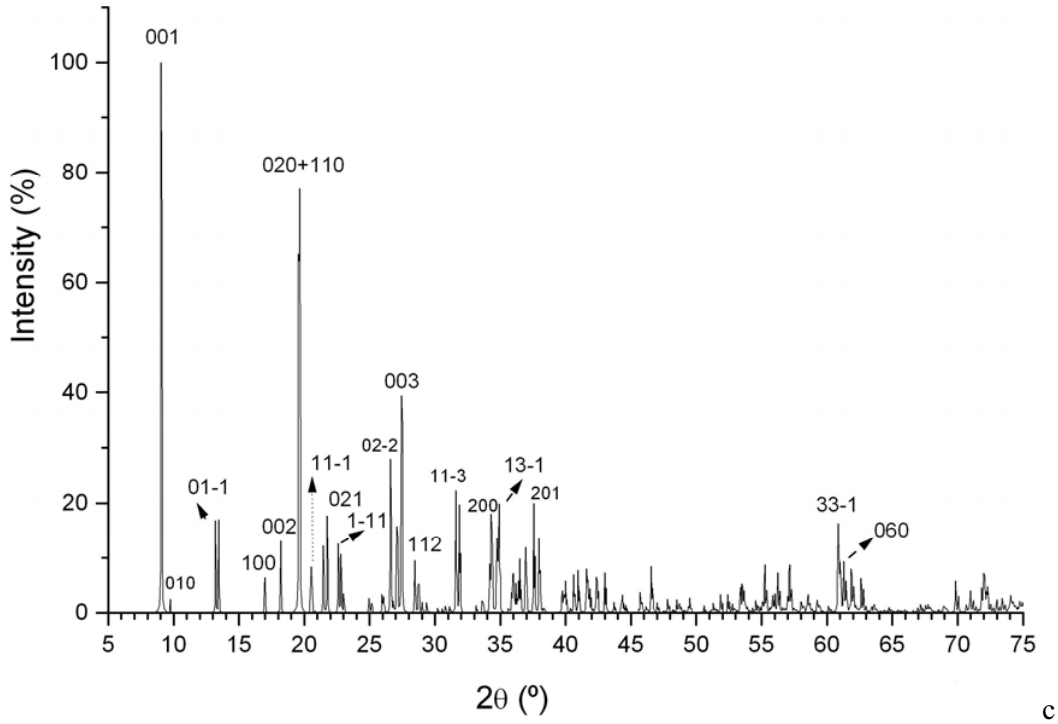
001
020+110
003
02-2
11-1
11-3
13-1
01-1
021
200
201
002
1-11
33-1
112
060
100
010
Intensity (%)
2θ (º)

c

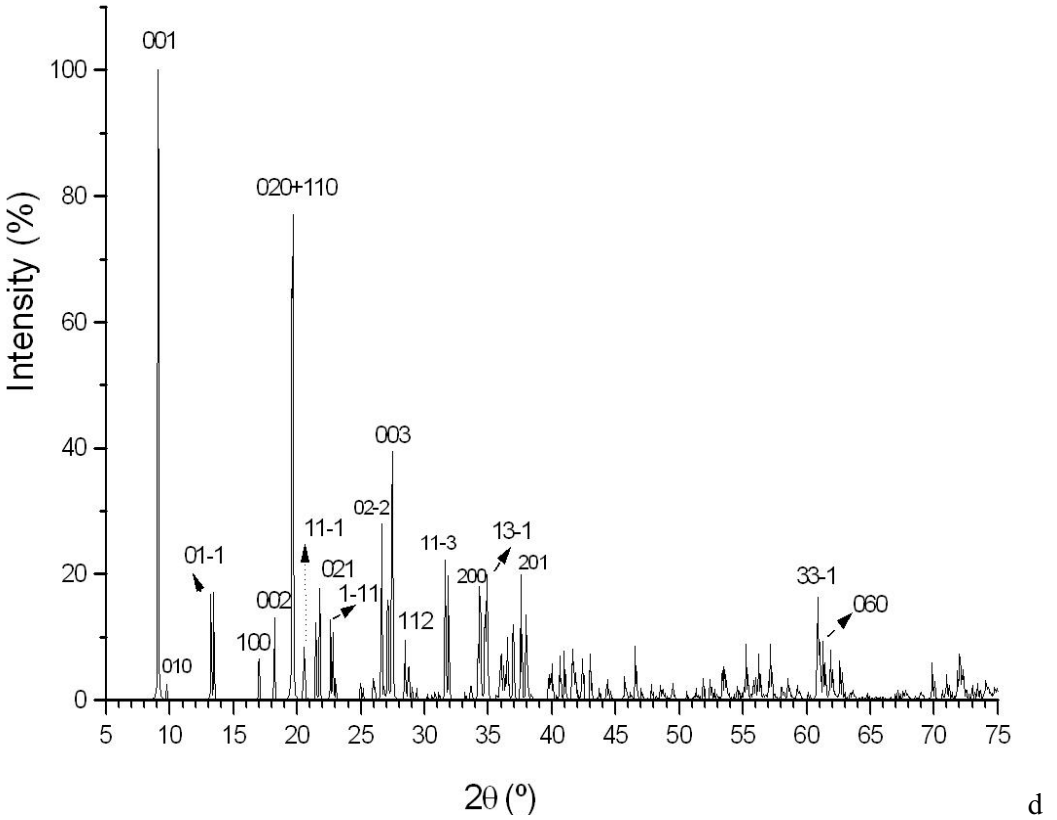
001
020+110
003
02-2
11-1
11-3
13-1
01-1
021
200
201
002
1-11
33-1
112
060
100
010
Intensity (%)
2θ (º)

d

Fig. 6

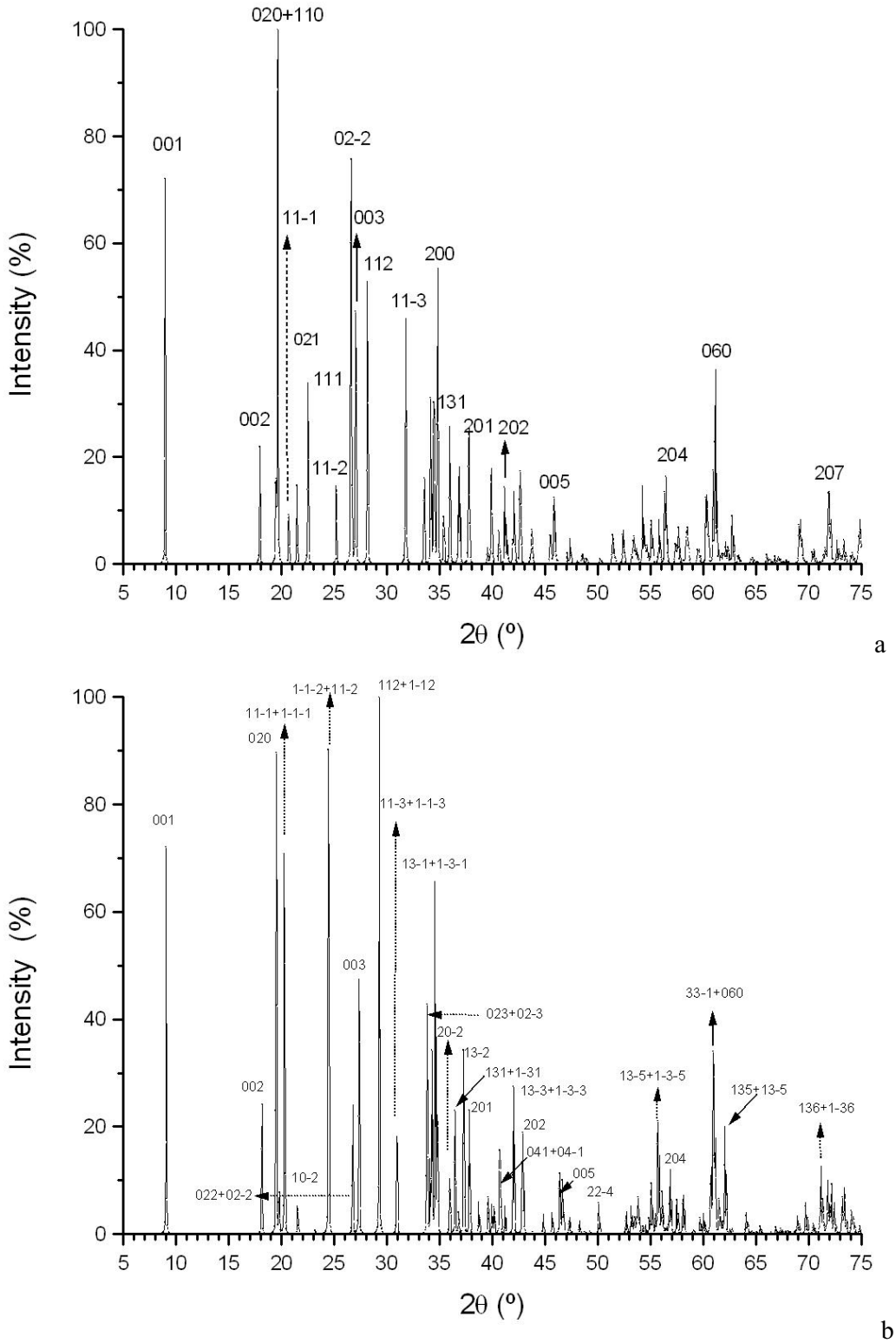
Intensity (%)
2θ (º)
020+110
001
02-2
11-1
003
112
200
11-3
021
060
111
131
002
201
202
204
11-2
005
207
a
1-1-2+11-2
112+1-12
11-1+1-1-1
020
11-3+1-1-3
001
13-1+1-3-1
003
023+02-3
33-1+060
20-2
13-2
131+1-31
13-5+1-3-5
135+13-5
002
13-3+1-3-3
201
136+1-36
202
041+04-1
204
10-2
005
022+02-2
22-4
b

Fig. 7

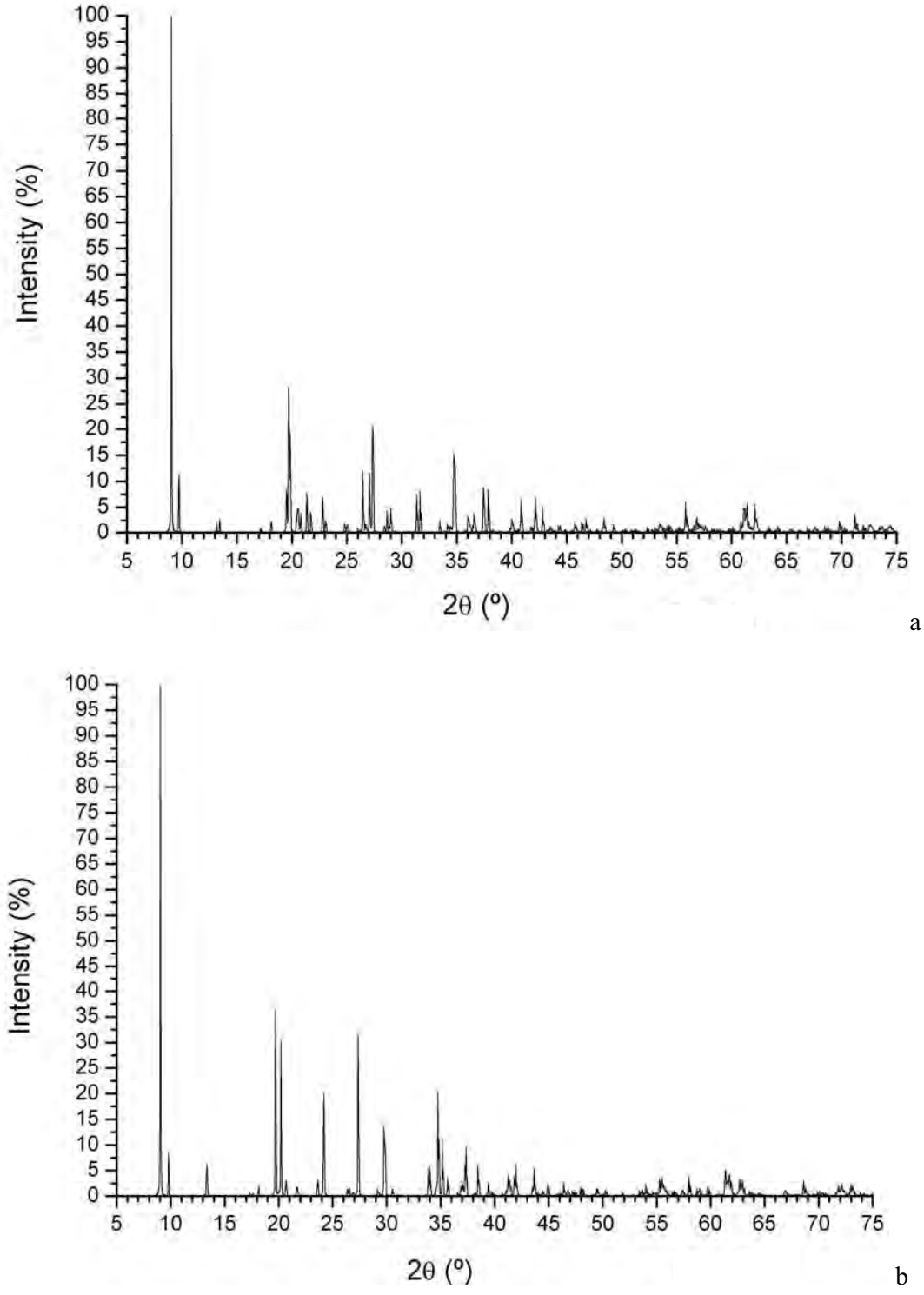

Fig. 8